BRITISH ANTARCTIC SURVEY

SCIENTIFIC REPORTS

No. 79

THE DYNAMICS OF THE BRUNT ICE SHELF, COATS LAND, ANTARCTICA

By

R. H. THOMAS, B.Sc., Ph.D.

British Antarctic Survey,
Scott Polar Research Institute, Cambridge

LONDON: PUBLISHED BY THE BRITISH ANTARCTIC SURVEY: 1973
NATURAL ENVIRONMENT RESEARCH COUNCIL

BRITISH ANTARCTIC SURVEY SCIENTIFIC REPORTS: No. 79

THE DYNAMICS OF THE BRUNT ICE SHELF, COATS LAND, ANTARCTICA

By

R. H. THOMAS, B.Sc., Ph.D.

British Antarctic Survey,
Scott Polar Research Institute, Cambridge

(Manuscript received 18th December, 1972)

ABSTRACT

OBSERVATIONS made during 1966–68 along a 70 km. flow line on the Brunt Ice Shelf are used to show that an average of 1 m. of ice is melted each year from beneath the ice shelf. Appreciable bottom melting occurs at all points along the flow line. Within the limits of observing errors, ice drainage into the ice shelf is found to balance surface accumulation over the catchment area. Particle trajectories indicate that snow falling at the hinge line takes about 190 yr. to reach the ice front and that, because of bottom melting, none of the snow falling at distances greater than 5 km. inland from the hinge line ever reaches the ice front. The high melting rates calculated at all points beneath the Brunt Ice Shelf suggest that bottom melting may be more widespread than previously suspected.

The behaviour of the Brunt Ice Shelf is largely influenced by the rapidly moving "Dalgliesh Ice Stream" which supplies the northern part of the ice shelf, where the ice front advances up to 1·5 km. each year. Farther south, ice movement is hindered by the grounded ice of the McDonald Ice Rumples. Between these two zones, large shear stresses have resulted in complete fracture of the ice shelf into isolated blocks separated by expanses of thin ice shelf, sea ice and leads that mark the lines of active separation. Large ice tongues may calve in response to tsunamis with a frequency equal to one of the natural frequencies of the ice tongue. Calving of long narrow ice tongues may be due to the prolonged action of stresses induced by sea currents.

CONTENTS

	PAGE
I. Introduction	3
II. The Brunt Ice Shelf	5
A. Morphology	5
B. Measurements	6
1. Accumulation	6
2. Ice movement	8
3. Strain-rates	11
4. Surface elevation and ice thickness	11
5. Other survey networks	11
a. Deformation at the hinge line	11
b. Growth rate of thin ice shelf	17
C. Discussion	17
1. Zone 1: rapidly moving ice shelf in the north	17
a. Strain-rates at the hinge line	19
b. Calving at the ice front	21
2. Zone 2	22
3. Zone 3	23
The McDonald Ice Rumples	24
III. The calving of icebergs	26
A. Existing theories	2
B. Influence of tsunamis on large ice tongues	27
C. Effects of sea currents on floating ice tongues	28
D. Hinge-line calving	29
IV. Mass balance, particle paths and bottom melting	31
A. Bottom flux	31
1. Non-steady-state bottom flux	34
2. Mean value of bottom flux over a large area	35
3. Influence of sea currents on bottom-melting rates	36
B. Mass balance of the inland ice sheet near the Brunt Ice Shelf	37
C. Particle paths	39
V. Conclusions and suggestions for further work	41
VI. Acknowledgements	42
VII. References	43

I. INTRODUCTION

ICE shelves are floating ice sheets, attached to an inland ice sheet or to land, that are nourished by snow accumulation and by the seaward extension of land glaciers. In exceptional circumstances the freezing of ice on to the bottom of the ice shelf is the main source of nourishment. According to Suyetova (1962), ice shelves represent about 10 per cent of the surface area of the Antarctic ice sheet, and it has been estimated (Bardin and Shil'nikov, 1960) that they act as outlets for more than half of the drainage from the inland ice sheet. Consequently, a knowledge of their behaviour is essential to any assessment of the mass balance of the ice sheet. Moreover, since ice shelves rest on water, their dynamics should be relatively easy to interpret.

The observations made on the Brunt Ice Shelf (Fig. 1)* are reported here but first the published work that forms the basis of our understanding of ice shelves will be reviewed.

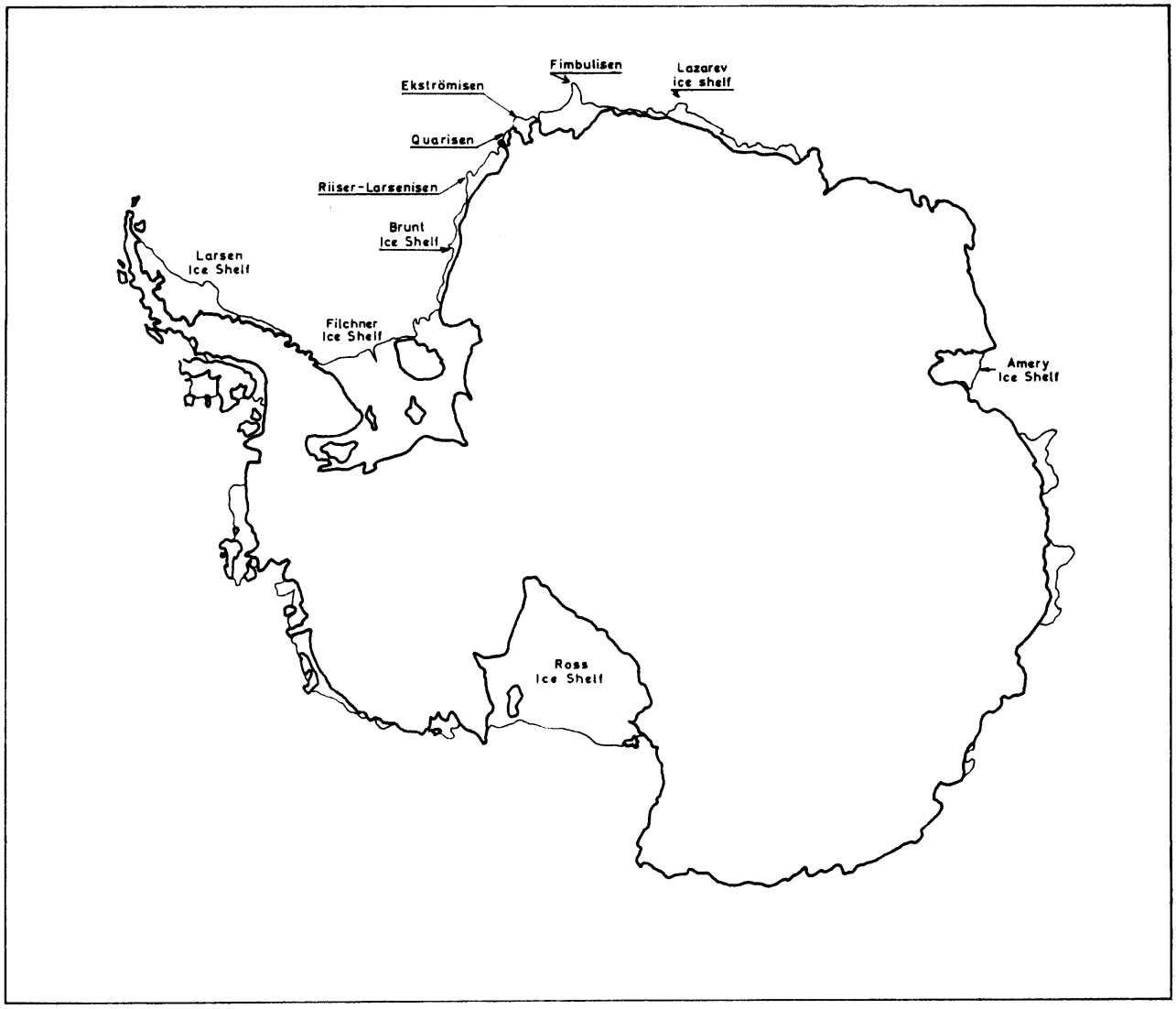

FIGURE 1

Map of Antarctica showing the locations of ice shelves referred to in the text.

* Quarisen in Fig. 1 will be referred to in the text as Maudheim ice shelf, since it has been much discussed in the literature under this name.

The most notable early contribution to our knowledge was that of Wright and Priestley (1922) in their report of the glaciological results of Scott's *Terra Nova* expedition. These writers considered ice shelves to be representative of the "zone of balanced forces" where snow accumulation is exactly compensated by spreading of the ice. In this way the ice-shelf thickness trends towards an equilibrium value determined by the temperature, accumulation rate and the extent to which the ice shelf is confined. A natural consequence of this process is the flat, relatively smooth upper surface which is the most characteristic feature of all ice shelves.

Very little was added to the work of Wright and Priestley until the Norwegian–British–Swedish Antarctic Expedition, 1949–52, attempted an extensive series of quantitative observations from their station on the Maudheim ice shelf. Robin (1958), using seismic sounding techniques, successfully measured ice-shelf thicknesses varying from 200 m. near the ice front to 500 m. near the inland margin of the Ekström ice shelf. Schytt (1958*a*, *b*) developed a method of interpreting the stratigraphy of Antarctic firn, and from observations in a 12 m. pit he inferred that the average accumulation rate at Maudheim for 1934–51 was 0·365 m. of water yr.$^{-1}$. This is in good agreement with the value for 1951 accumulation obtained from stake measurements (Swithinbank, 1957*b*). To investigate the inner structure of the ice shelf, cores recovered from a 100 m. bore hole were examined for density variations, crystal size and *c*-axis orientation (Schytt, 1958*b*). Temperature measurements in the hole (Schytt, 1960) showed a gradual but accelerating increase with depth. Swithinbank (1957*a*), as a result of a careful examination of the morphology of the ice shelves near Maudheim, concluded that their seaward limits were dependent on the existence of shoals which could ground the ice. Thus, analysis of present-day sea depths could establish the probable seaward limits of an ice shelf under conditions of more intense glacierization. Swithinbank (1958) also measured the rate of spreading of the ice shelf and, by balancing this against snow-accumulation rate, concluded (Swithinbank, 1960) that 0·9 m. of ice yr.$^{-1}$ were melted from the bottom of the ice shelf.

At this stage there was a strong need for a theoretical model with which the observations could be compared, and the work at Maudheim provided the stimulus for the interpretations of ice-shelf creep (Weertman, 1957; Robin, 1958, p. 114) and of temperature distribution (Robin, 1955, 1959; Wexler, 1960) which closely followed the publication of the expedition's results.

During the International Geophysical Year (1957–58) work similar to that completed at Maudheim was attempted on both the Filchner Ice Shelf (Behrendt, 1962) and Ross Ice Shelf (Crary, 1961; Crary and others, 1962). In addition, a hole was bored completely through the Ross Ice Shelf (Bender and Gow, 1961). Despite many attempts, it has so far proved difficult to obtain a satisfactory match between the observed and theoretical distributions of temperature with depth (Robin, 1955; Wexler, 1960; Crary, 1961; Jenssen and Radok, 1961; Zotikov, 1964).

By comparing available measurements of the rate of outflow of ice across the major ice fronts with snow-accumulation rates on the inland ice sheet of Antarctica, Giovinetto (1970) concluded that, whilst the mass balance of the interior of the continent is positive, that of the peripheral region is larger and negative. However, the errors involved in Giovinetto's estimates are large, due in part to uncertainty regarding the amount of ice lost by melting (or gained by freezing) beneath the ice shelves. The measurements of the Brunt Ice Shelf described in this report were used by Thomas and Coslett (1970) to estimate bottom-melting rates along a profile right across the ice shelf. These showed that there is appreciable melting ($\sim$ 1 m. ice yr.$^{-1}$) at all points along a 70 km. flow line despite the probable shallow depth of sea-water beneath the ice shelf. Observations reported by Behrendt (1970) imply larger melting rates beneath the Filchner Ice Shelf, under which the layer of sea-water is considerably thicker. These conclusions provide evidence for more widespread bottom melting than previously suspected, and they may imply a net increase in world ocean mass.

Apart from its immediate relevance to the mass balance of an ice shelf, the bottom-melting rate influences the temperature distribution within the ice shelf and this in turn determines the values of the flow parameters of the ice. Because the behaviour of an ice shelf can be well approximated by that of a mathematically tractable model, the observations of ice-shelf creep rates can be used to deduce these parameters. Thomas (1971, 1973*a*, *b*) used available measurements to calculate the flow-law parameters for several ice shelves at stresses lower than can reasonably be studied in the laboratory. The results show good agreement with values extrapolated from laboratory work.

II. THE BRUNT ICE SHELF

THE position of the British Antarctic Survey station at Halley Bay on the Brunt Ice Shelf offered an excellent opportunity for studying ice-shelf problems. The amount of snow accumulation near the station has been intermittently recorded by stake measurements and pit observations since it was first occupied in 1956. More detailed work including attempts to measure the velocity and strain-rates at the surface of the ice shelf was completed in 1956–59 and 1960–61 (Limbert, 1963, 1964; MacDowall, 1964; MacDowall and others, 1964; Ardus, 1965*a*, *b*). The work reported here results from a 3 year field programme begun in 1966. It was planned to provide information from a number of widely scattered stations on the ice shelf and to attempt detailed investigations of specific problems: mass balance at the bottom of the ice shelf; particle trajectories through the ice shelf; the creep of ice at low stresses; and the formation *in situ* of new ice shelf between blocks of older ice shelf. The general results are presented here; detailed reports on individual topics are listed in the references.

A. MORPHOLOGY

The Brunt Ice Shelf is one of several small ice shelves fringing the east coast of the Weddell Sea. The history and morphology of the area have been well described by Limbert (1963), Barclay (1964) and Ardus (1965*a*, *b*). However, recent American air photographs of the area in conjunction with observations made during journeys over the surface enable a more accurate description to be made of the limits and features of the ice shelf (Fig. 2). It forms a 50–150 km. wide fringe extending in a north-easterly direction along the Caird Coast from the "Dawson-Lambton Ice Stream" at lat. 76° 07' S., long. 27° 00' W., to "Christmas Box Ice Rise" at lat. 74° 20' S., long. 20° 30' W. The ice shelf is at its widest in the north where it fills a large bight in the Caird Coast and is supplied by the large and active "Dalgliesh Ice Stream" which drains the area to the west of Heimefrontfjella. Where the ice stream becomes afloat a zone of severe crevassing extends about 50 km. into the ice shelf (Plate I).

Farther west, movement of the ice shelf is confined by a small area of grounded ice, the McDonald Ice Rumples. Between this area and the rapidly moving ice associated with the "Dalgliesh Ice Stream" the ice shelf is severely fractured, and large expanses of thin new ice shelf have formed between isolated blocks of thicker ice shelf (Plate IIa). The seaward limits of the ice shelf are broadly determined by the positions of two areas of grounded ice, an example of the general principle postulated by Swithinbank (1957*a*, p. 34) that the stable configuration of an ice shelf is defined by the outermost shoals which could ground it.

The surface of the ice shelf is nowhere completely flat; it consists of a series of waves of about 1 km. wave-length and 5 m. wave height. Up-stream from the McDonald Ice Rumples there are pressure waves which noticeably increase in frequency and wave height near the ice rise. To the south and south-east of the McDonald Ice Rumples, the junction (or hinge line) between ice shelf and inland ice sheet is marked by a 10–20 km. wide belt of disturbed ice. As the hinge line is approached the surface becomes more and more steeply undulating, and the ridges finally become recognizable as icebergs, calved from the inland ice sheet and subsequently streamlined by the accumulation of drift snow (Plate IIb). Near the hinge line, the north cliff-like faces of these ridges are far steeper than the relatively gentle south slopes, and oval basins aligned parallel with the prevailing east–west wind have formed beneath the cliffs. Similar features occur on the Lazarev ice shelf and have been named deflation basins by Konovalov (1963). They form where differential ablation by wind erosion and insolation is able to modify the surface relief.

To the west of each of the ice rises the ice front is incised by huge rifts. Near the McDonald Ice Rumples (Plate IIIa and b), these range in length from a few hundred metres to 3 km., whilst those near "Christmas Box Ice Rise" extend for several tens of kilometres with widths up to 3 km. They are floored with sea ice and heavy accumulations of drift snow. Actively opening rifts can be distinguished from others by the presence of expansion cracks in the sea ice. Their activity decreases with increasing movement down-stream from the grounded ice, and they finally degenerate into narrow inlets in the ice front leading to long ramps of snow. These provide easy access to the surface of the ice shelf, and it was their presence near the McDonald Ice Rumples that decided the position of the Halley Bay station. Between the inlets, headlands have evidently been upwarped by the buoyancy of submarine rams of ice as described by Swithinbank (1957*a*, p. 14).

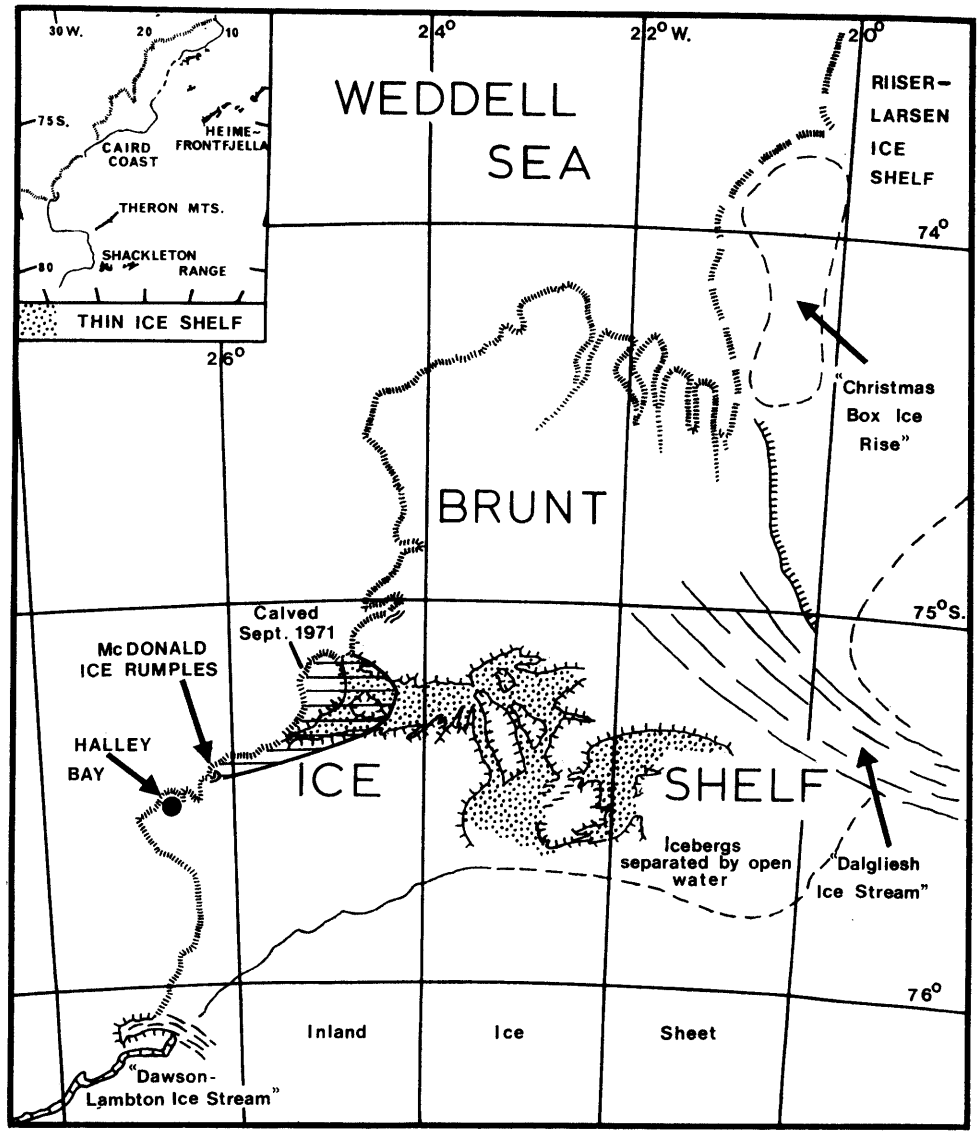

FIGURE 2
Map of the Brunt Ice Shelf.

B. MEASUREMENTS

1. *Accumulation*

Snow-accumulation rates were obtained by measuring the lengths of stakes planted in the snow surface. Route markers and ice-movement stations were also used for this purpose, giving accumulation rates over a wide area of the ice shelf and adjacent inland ice sheet. Measurements were made once or twice each year, though more frequently near the station and along well-travelled routes, but no attempt was made to study short-period accumulation rates. Snow pits were examined at a number of sites but interpretation of the annual stratification was seldom sufficiently unambiguous to supply reliable accumulation rates.

The stakes were made of aluminium tubing 25 mm. in diameter with a wall thickness of 1·6 mm. Sections 2 m. long were plugged at the bottom end to minimize sinking and were fitted with extension sockets at the top. In each case a double length was planted to a depth of approximately 1 m. and additional sections were added whenever the exposed length became less than 2 m. The stake measurements give an estimate of the apparent depth of snow accumulated since the measurements began. This differs from the true value by the amount of settling in the snow layers between the original surface and

the point at which the stake is anchored to the surrounding snow. To test where the accumulation stakes were anchored, comparison was made between data obtained from a standard stake and one barbed at its base, thus anchoring it to the snow layers around the stake bottom. There were no significant differences between the results, and all stake measurements have been interpreted on the assumption that stakes were fixed at the base.

The true depth of accumulation then becomes the apparent depth plus the compaction due to settling of the snow between the original surface and the stake bottom. Settling rates can be measured directly by comparing stakes planted to different depths, or they can be inferred from the depth/density curve for the surface snow and firn. In areas of little or no melting, Sorge (1935) observed that the distribution of density with depth at any point was independent of time. Also, in the absence of melting and lateral strain, the mass of any snow layer remains constant. Thus:

$$\int_{h}^{h+\Delta h} \rho \mathrm{d}h = \text{constant} \tag{1}$$

$$\text{or } \bar{\rho}\Delta h = \text{constant}, \tag{1a}$$

where $\bar{\rho}$ is the mean density of the snow layer between depths h and $h + \Delta h$; in the present case between the original snow surface and the bottom of the stake. As h increases with time the compaction in that layer becomes:

$$\Delta h - \Delta h' = \Delta h\left(1 - \frac{\bar{\rho}}{\bar{\rho}'}\right), \tag{2}$$

where the primed values are those after compaction. Using this expression and values of $\bar{\rho}$ from the depth/density curves from three pits, settling corrections were applied to all stake measurements, and corrected snow depths were converted to equivalent depths of water.

The available measurements of snow accumulation near Halley Bay are shown in Fig. 3; those prior to 1956 are the mean values from two pits (MacDowall, 1964; Ardus, 1965*a*, *b*). The mean of the whole

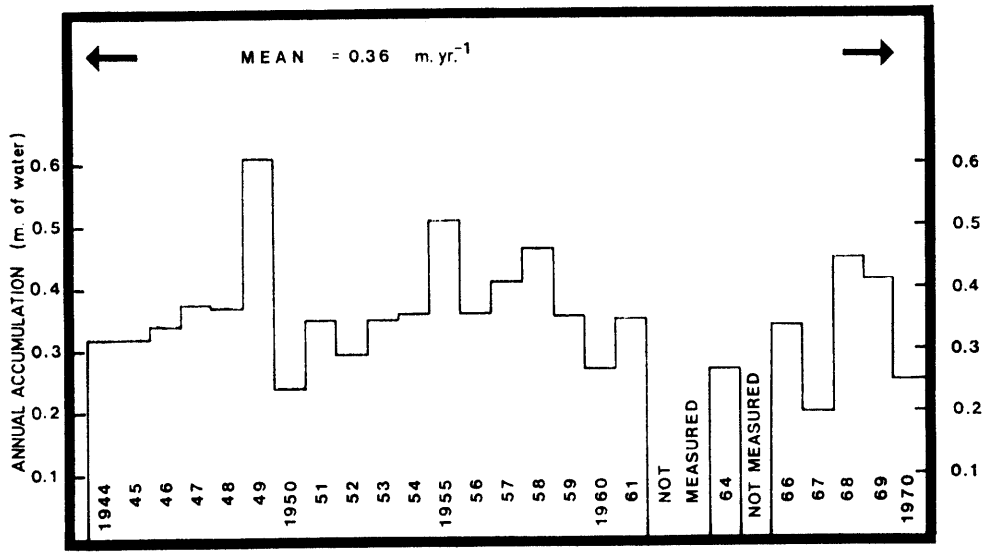

FIGURE 3

Snow-accumulation rate near Halley Bay station plotted against time.

period (1943–69) gives an annual accumulation rate ($\dot{A}_1$) which is likely to be more typical than that for 1966–69 ($\dot{A}_2$). However, during the shorter period, accumulation was measured over larger areas of the ice shelf and the adjacent inland ice sheet. The values obtained were adjusted by multiplying each by $\dot{A}_1/\dot{A}_2$, assuming that the accumulation pattern revealed by the short-period data would be retained over longer periods. Fig. 4 shows an accumulation-rate profile extending from the ice front across the ice shelf and on to the inland ice sheet. A rapid decrease in accumulation near the ice front has been

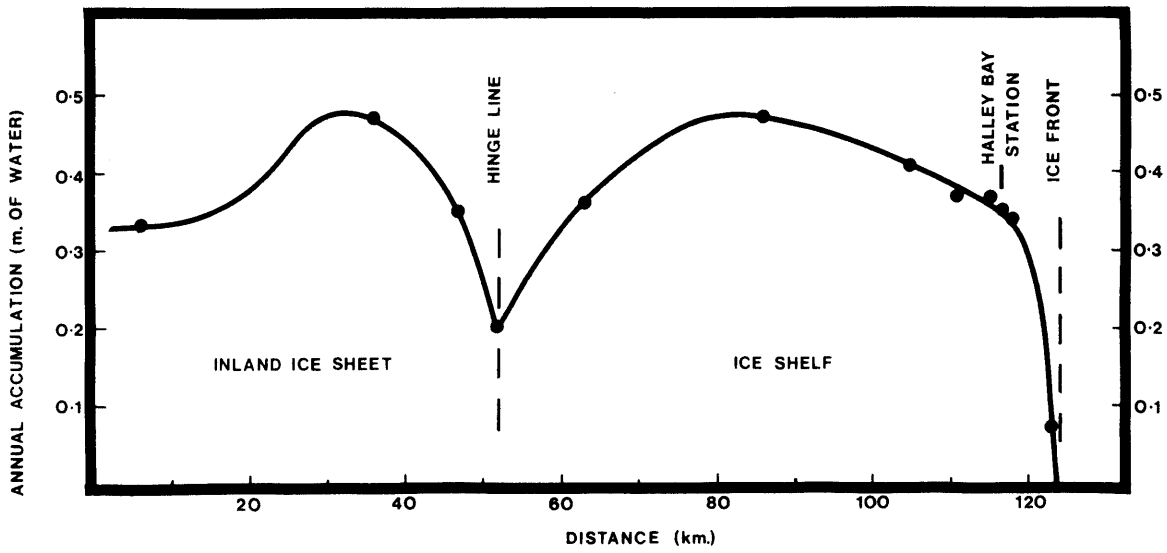

FIGURE 4

Snow accumulation-rate profile along the flow line through Halley Bay station.

observed on other ice shelves; Kruchinin (1965, p. 87) gave data from the Lazarev ice shelf indicating ablation within 15 m. of the ice front and reduced accumulation rates within 500 m. of the ice front. The Brunt Ice Shelf measurements indicate that the zone of diminished accumulation near the ice front is from 4 to 5 km. wide, whilst Swithinbank (1957*b*, p. 45) found the equivalent distance for the Maudheim ice shelf to be 1–2 km. The most likely reason is increased wind scour near the ice front, the width of the zone affected being dependent on the strength and direction of prevailing winds.

A reduction in accumulation near the junction between the inland ice sheet and ice shelf has been observed both on the Maudheim and Fimbul ice shelves (Swithinbank, 1957*a*, p. 17; Lunde, 1961, p. 42). Katabatic winds from the inland ice sheet reduce the accumulation rate both on the steeper land-ice slopes and over a narrow zone on the ice shelf. This is well illustrated by the observations of Lunde at the foot of the continental slope on Fimbulisen, where snow accumulation during the spring and summer katabatic winds dropped to 3 per cent of that at Norway Station on the ice shelf. However, on the Brunt Ice Shelf there is a high rate of drift-snow accumulation between the icebergs that form at the hinge line. This is not reflected in the accumulation measurements, which were made on the tops of icebergs.

2. *Ice movement*

The complete absence of rock outcrops within several hundred kilometres of Halley Bay limits the survey techniques that can be applied to deduce the absolute movement of the ice shelf. These are:

i. *Comparison of astro-fixes.* From 1956 to 1970 the position of Halley Bay was fixed annually. Although the errors in individual fixes were large (± 100 m.), the mean ice velocity implied by the first-order regression line through the fixes has a random error of ± 25 m. yr.$^{-1}$.

ii. *Repeated magnetic surveys.* The position of a north–south orientated magnetic anomaly relative to stations on the ice shelf was accurately mapped in 1960 (Blackwell, 1960) and again in 1969 (personal communication from J. Jamieson). It probably represents the most accurate method for determining absolute velocity on the ice shelf, and it is hoped that regular measurements will detect any variations in velocity.

iii. *Repeated mapping.* Using grounded icebergs as fixed control points, Limbert (1964) and Ardus (1965*a*, *b*), repeatedly mapped the positions of stations on the ice shelf. Comparison of the surveys gave an estimate of ice-shelf movement. Unfortunately, of the several icebergs observed, only one could be used as a control point for the two surveys made by each observer, and the stated

errors covered neither the possible movement of the icebergs nor weathering of the feature observed. Because the iceberg used by Ardus was one which Limbert had earlier suspected of movement (personal communication from D. W. S. Limbert), his results are not included in this work.

These three independent methods give a measure of the absolute movement of a point on the ice shelf (Table I). By incorporating this point within a survey scheme designed to measure relative movement,

TABLE I

COMPARISON OF INDEPENDENT ESTIMATES OF ICE VELOCITY AT HALLEY BAY STATION

Source	*Interval*	*Annual velocity and direction*	
		m. yr.$^{-1}$	*East of true north*
i	1957–70	396±25	266°±5°
ii	1960–69	420±20	270°±5°
iii	1959	366±40	266°±5°
Thomas, assuming the grounded ice to be stationary	1966–67	349± 2	272°±2°

control was transferred across the ice shelf and estimates of absolute velocity were obtained for all the survey stations. The grounded ice of the McDonald Ice Rumples was chosen as origin of the relative-movement grid, which consisted of a triangulation network of linked and braced quadrilaterals of side length 3–5 km. extending from the ice front near Halley Bay across the ice shelf and on to the inland ice sheet 60 km. to the south-east (Fig. 5). The necessary observations were completed in 1966 and 1967. Each survey occupied two men working with a small motor toboggan for a period of 3 months, in the course of which the survey figures suffered continual distortion and thus, without adjustment, failed to "close" by several minutes of arc. Faced with a similar problem, Swithinbank (1958, p. 86) reduced by linear interpolation all observed angles and measured lengths to two epoch dates, and then processed the two sets of data independently. Although sufficiently accurate where strain-rates are small, this method gives large errors in areas of rapid shearing. A better approximation was that adopted by Dorrer (Dorrer and others, 1969), who assumed that the ice velocity at any point on the ice shelf was constant over the period of the survey. This technique was applied to the Brunt Ice Shelf survey which was solved as a series of resections with the epoch-reduced coordinates of observed stakes as control points (Thomas, 1970). In this way two position fixes corresponding to the times of occupation were obtained for each stake. Comparison of these fixes gave a velocity relative to the origin of the survey on the McDonald Ice Rumples. Errors reached a maximum on the inland ice sheet: ± 3·5 m. yr.$^{-1}$ and ± 3° of arc.

In Table I the velocity obtained by this method for the Halley Bay station is compared with the estimates of absolute velocity, the mean of which is larger by 50 m. yr.$^{-1}$. Little is known about possible annual variations in velocity during the period covered by the observations, but they are not likely to be sufficiently large to account for this difference, which is believed to be due to movement of the grounded ice of the McDonald Ice Rumples and hence of the origin of the relative-movement survey. To correct for this the movement vectors at each stake have been adjusted for an assumed ice velocity at the McDonald Ice Rumples of 50 m. yr.$^{-1}$ to the west (Fig. 6a). Before this correction was made the apparent movement vectors on the inland ice sheet were inclined about 40–50° to the form lines, whereas in Fig. 6a they are perpendicular, which is in accordance with predictions from theory (Nye, 1952, p. 92) and is a further indication that the velocity assigned to the McDonald Ice Rumples is approximately correct.

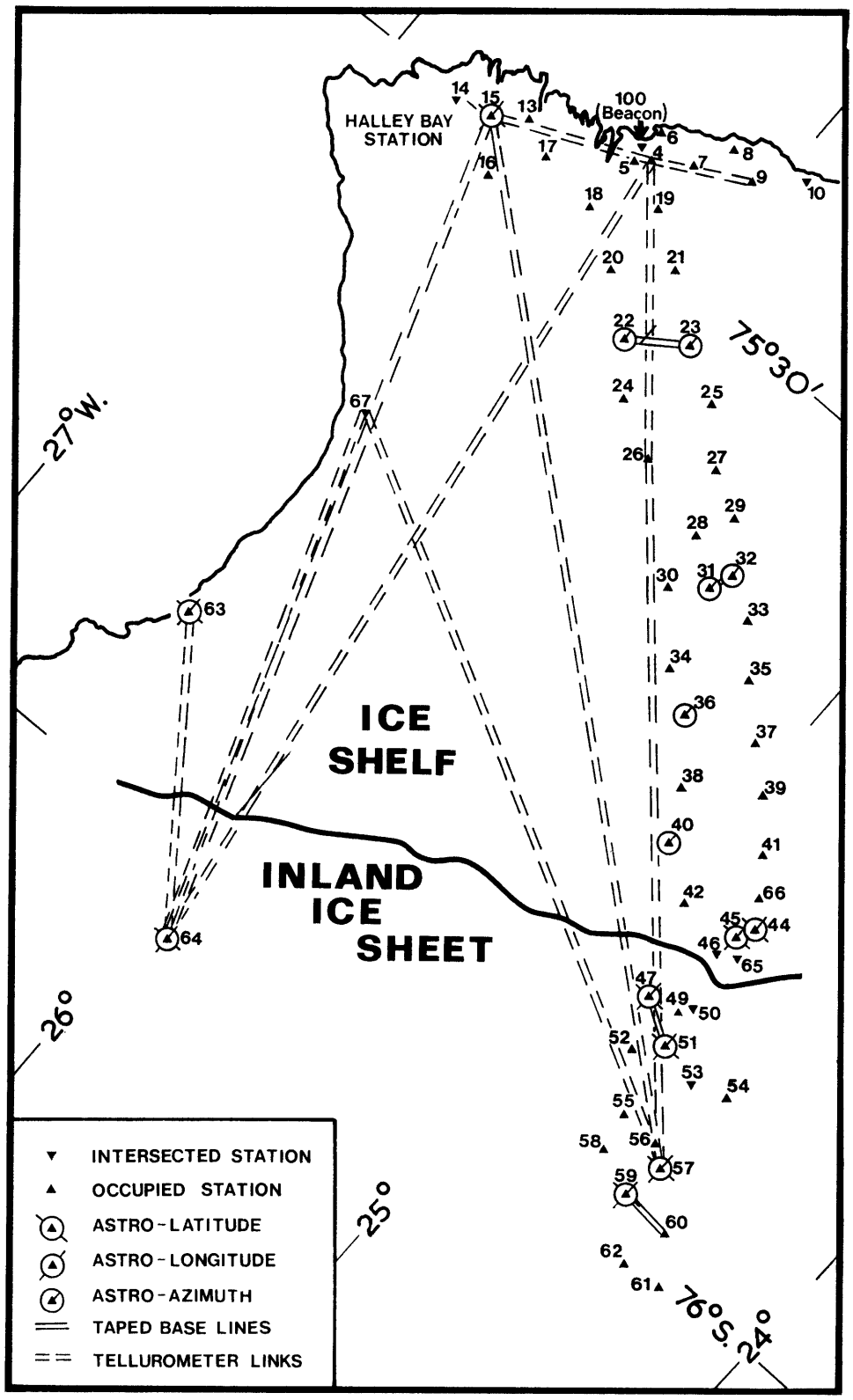

FIGURE 5

Survey network on the Brunt Ice Shelf and adjacent inland ice sheet.

3. *Strain-rates*

Principal strain-rates at the surface can be found for any triangle in which the relative velocities of the apices are known, and hence for any stake triangle within the relative-movement grid. Strain-rates were calculated as:

$$\dot{\epsilon} = \frac{1}{\Delta T} \log_e \left(\frac{L_2}{L_1}\right) \tag{3}$$

with L_1 = length at time T_1, L_2 = length of time T_2, $\Delta T = T_2 - T_1$ and $\Delta L = L_2 - L_1$, and for small $\Delta L/L_1$ this reduces to:

$$\dot{\epsilon} \sim \frac{\Delta L}{L_1 \Delta T}. \tag{4}$$

A selection of principal strain-rates is shown in Fig. 6b; small triangles formed from adjacent stakes have been used and the results plotted at the centre of the triangle, although they actually refer to the strain-rates over the triangle as a whole rather than at a point. The accuracy of the survey implies a strain-rate accuracy of $\pm 4 \times 10^{-5}$ yr.$^{-1}$.

In Fig. 7 the information gained from the triangulation network is summarized together with strain-rates and ice velocities obtained from isolated stake rosettes of the type described by Kehle (Zumberge and others, 1960, p. 75). They consisted of three stakes forming a 60° triangle with a fourth central stake. The distance from centre to apices was usually 360 m. but in two cases it was 100 m. Absolute velocities of the central stake and rates of twist of the entire rosette were deduced from repeated astronomical observations. At least once each year distances and angles were observed from the central stake to all corner stakes, and their rates of change were used to compute the principal strain-rates. Careful measurement kept the observing errors below 1 part in 30,000. In addition, tilting of the stakes introduced an "index" error to all measured lengths; the error carried in this way to the strain-rates is inversely proportional to the size of the rosette. Consequently, the smaller rosettes were unlikely to be adequate in areas of low strain where the errors became comparable with the measured strain-rates. The two on the Brunt Ice Shelf (R1 and R3 in Fig. 6b) were superimposed within larger rosettes. The results from R1, situated in an area of low strain-rate ($<10^{-3}$ yr.$^{-1}$), differ sufficiently from the larger rosette to invalidate them. R3, however, was planted in an area suffering intense deformation and its results adequately represent the local strain-rates.

By comparing the distribution of crevasses on the ice shelf and inland ice sheet with the measured strain-rates, a value is obtained for the critical strain-rate associated with fracture, $\dot{\epsilon}_c$, of approximately 6×10^{-3} yr.$^{-1}$ for ice with a 10 m. temperature of −19° C. This falls between the values reported by Holdsworth (1969*a*) of $\dot{\epsilon}_c \sim 2 \times 10^{-3}$ yr.$^{-1}$ and $1{\cdot}3 \times 10^{-2}$ yr.$^{-1}$ for ice with 10 m. temperatures of −28° and 0° C, respectively.

4. *Surface elevation and ice thickness*

In 1967–68 and again in 1970–71 the surface of the ice shelf was accurately levelled along a 70 km. line which extended through the ice-movement markers from the ice front to the junction between the ice shelf and inland ice sheet. The profile is shown in Fig. 8a together with ice-thickness measurements made along the same route by airborne radio echo-sounding (Evans and Smith, 1970). A second surface profile (2 in Fig. 8a) was levelled along a route taken approximately across the direction of flow. The levelling routes are shown in Fig. 8b.

5. *Other survey networks*

a. *Deformation at the hinge line.* A small, independent survey scheme designed to measure the behaviour of the ice shelf at the line of flotation was positioned midway between stakes 63 and 64. All stations were intersected from each end of an 800 m. base line and the orientation of the survey was controlled by astronomical observations of true azimuth. 1 year separated the two surveys, each of which was completed in 2 days, so reduction to epoch by linear interpolation of the observed angles introduced negligible errors. Using the epoch-reduced angles, triangles were solved by the sine formula assuming the Earth's surface to be plane. Comparison of the positions obtained from each survey led to the stake velocities shown in Fig. 9 relative to one of the stakes (B13) on the inland ice sheet. Assuming

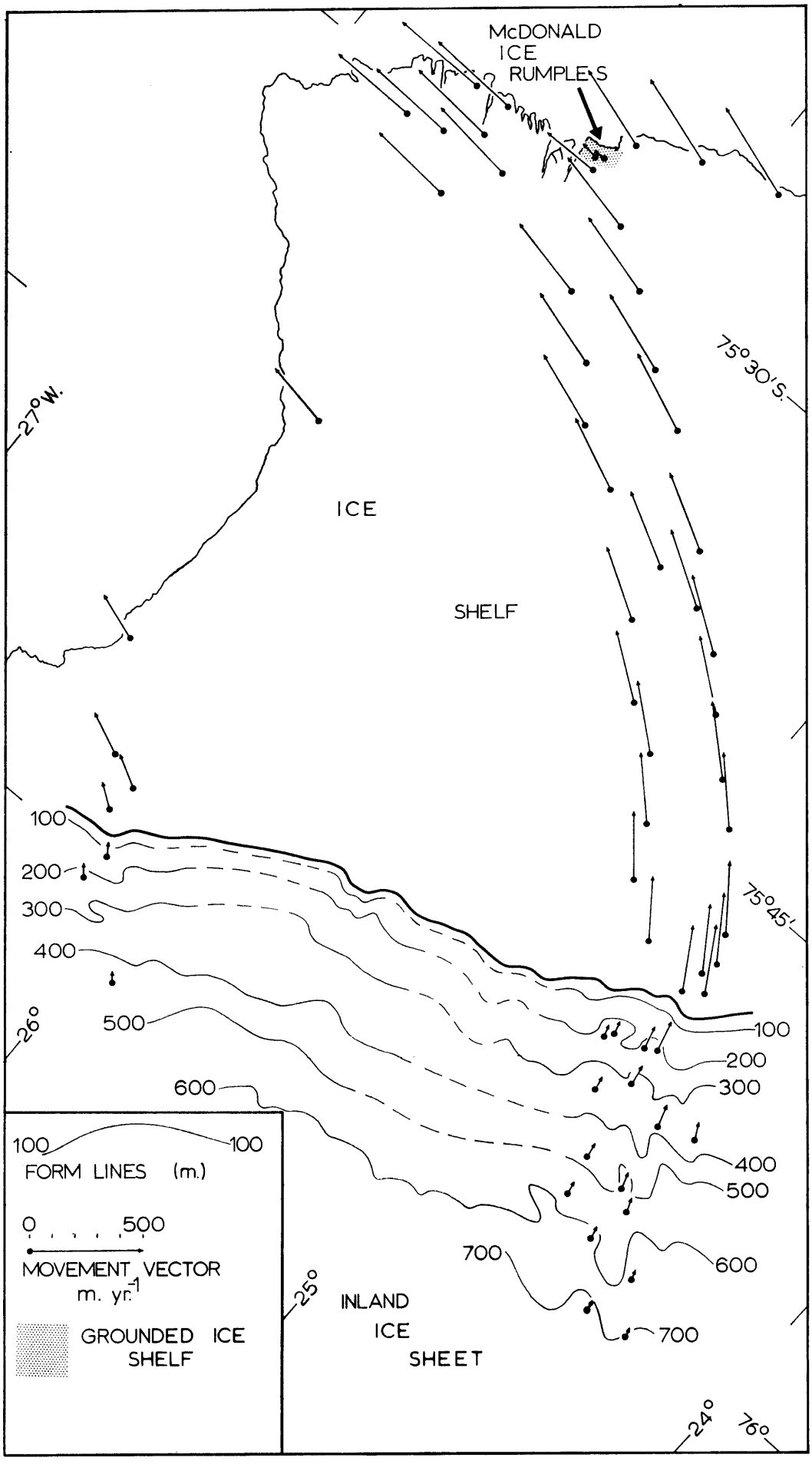

FIGURE 6

a. Ice-movement vectors on the Brunt Ice Shelf and adjacent inland ice sheet.

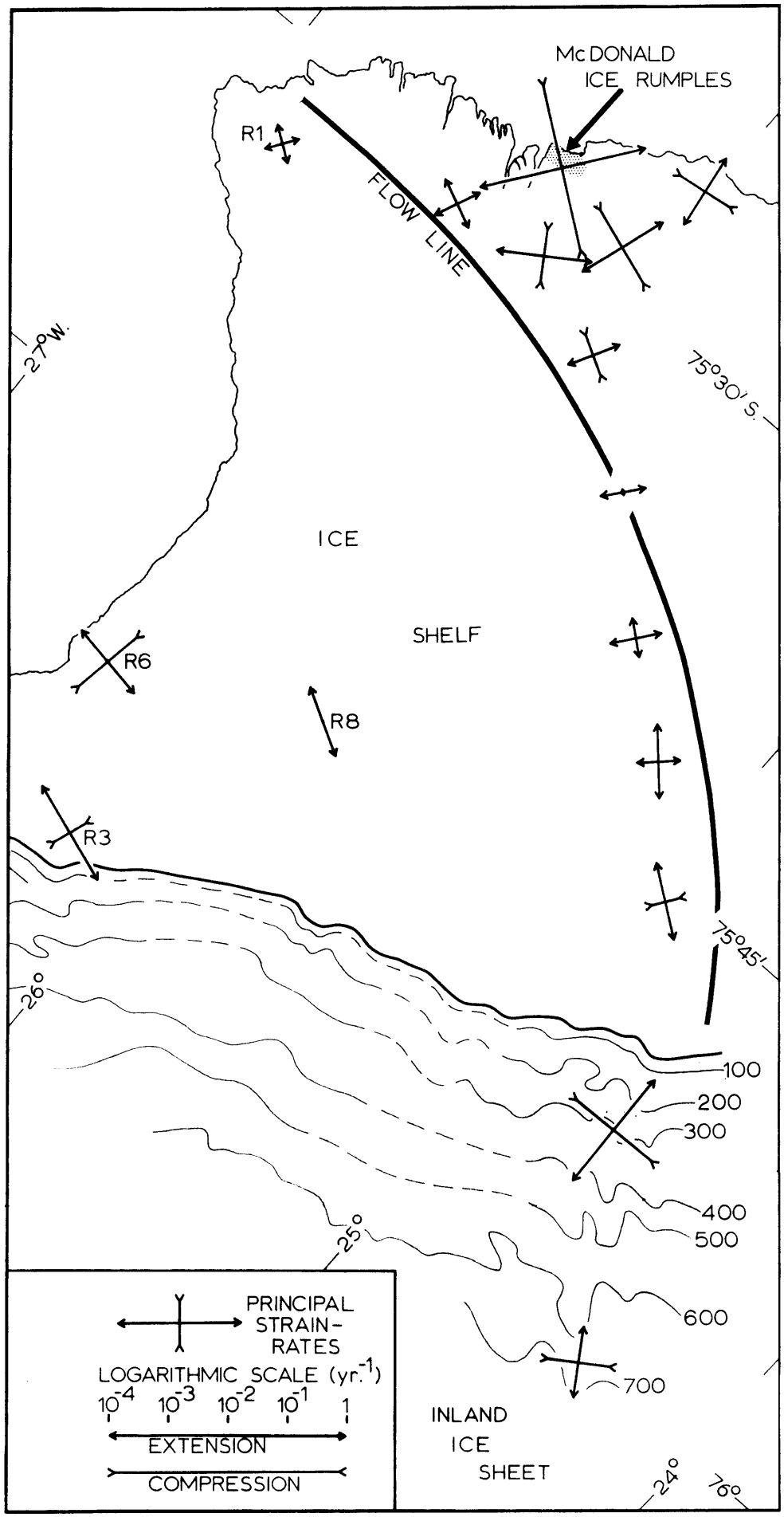

FIGURE 6

b. A selection of principal strain-rates deduced from the ice velocities illustrated in Fig. 6a. Values at R1–R8 were obtained from strain rosettes.

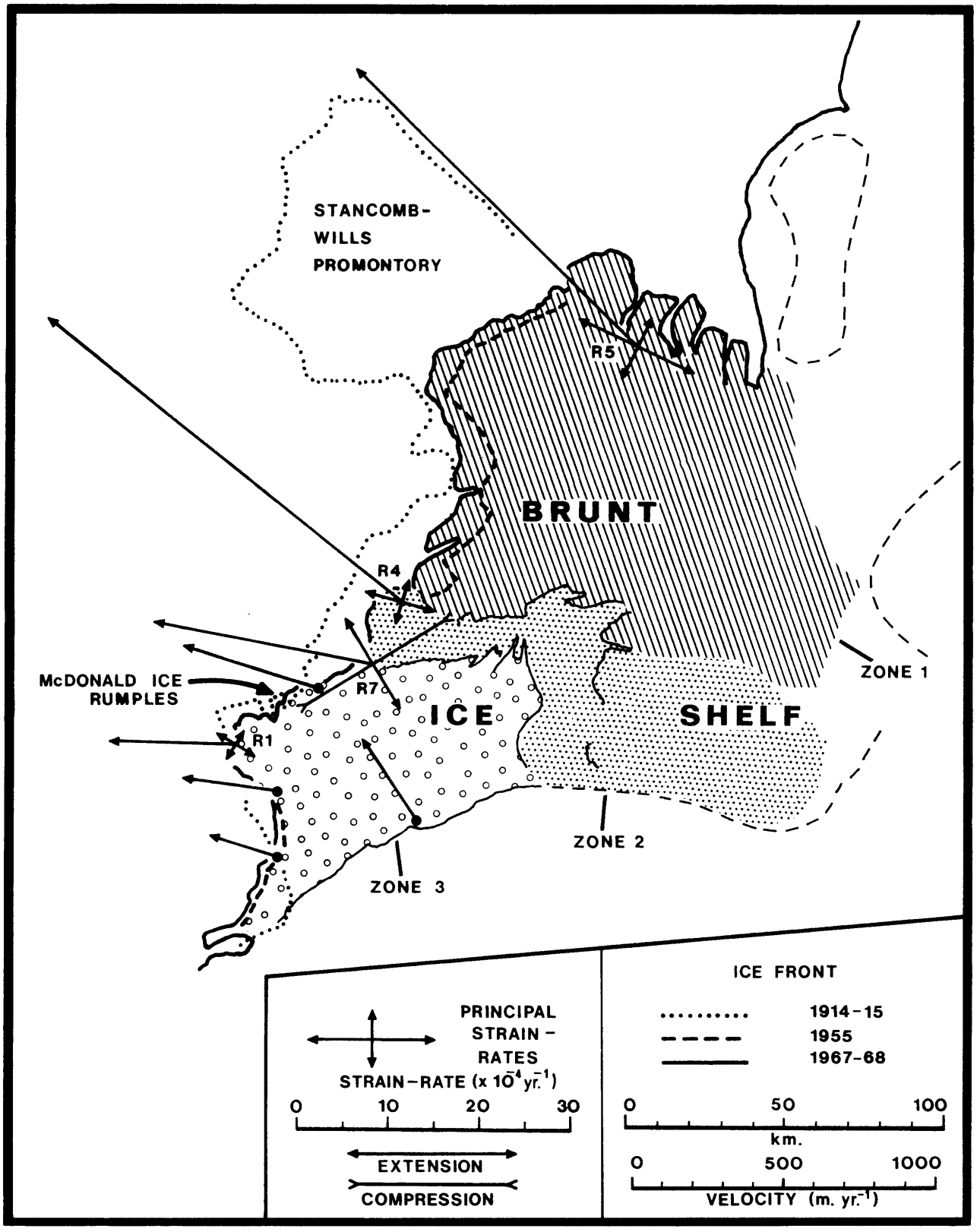

FIGURE 7

Three plots of the Brunt Ice Front, showing major changes which took place between 1914 and 1968. A selection of movement vectors and principal strain-rates is also shown.

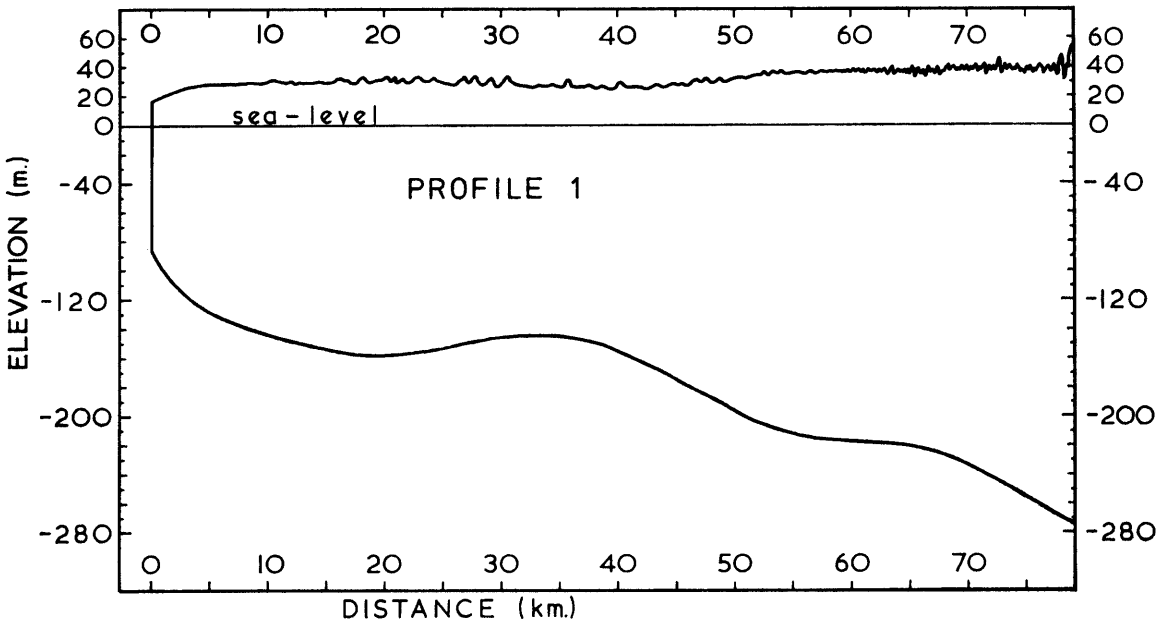

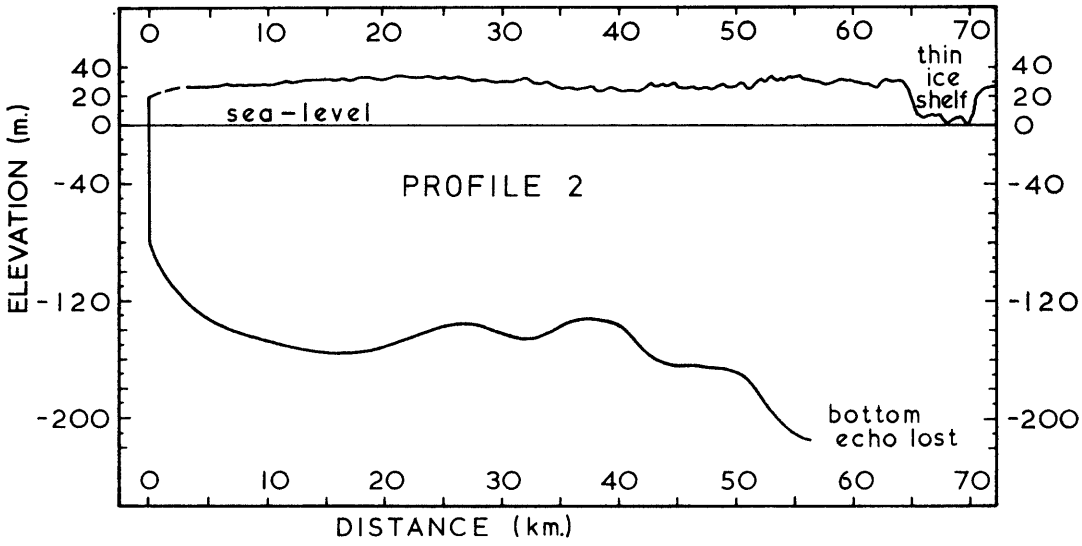

FIGURE 8

a. Ice-thickness and surface-elevation profiles for the Brunt Ice Shelf.

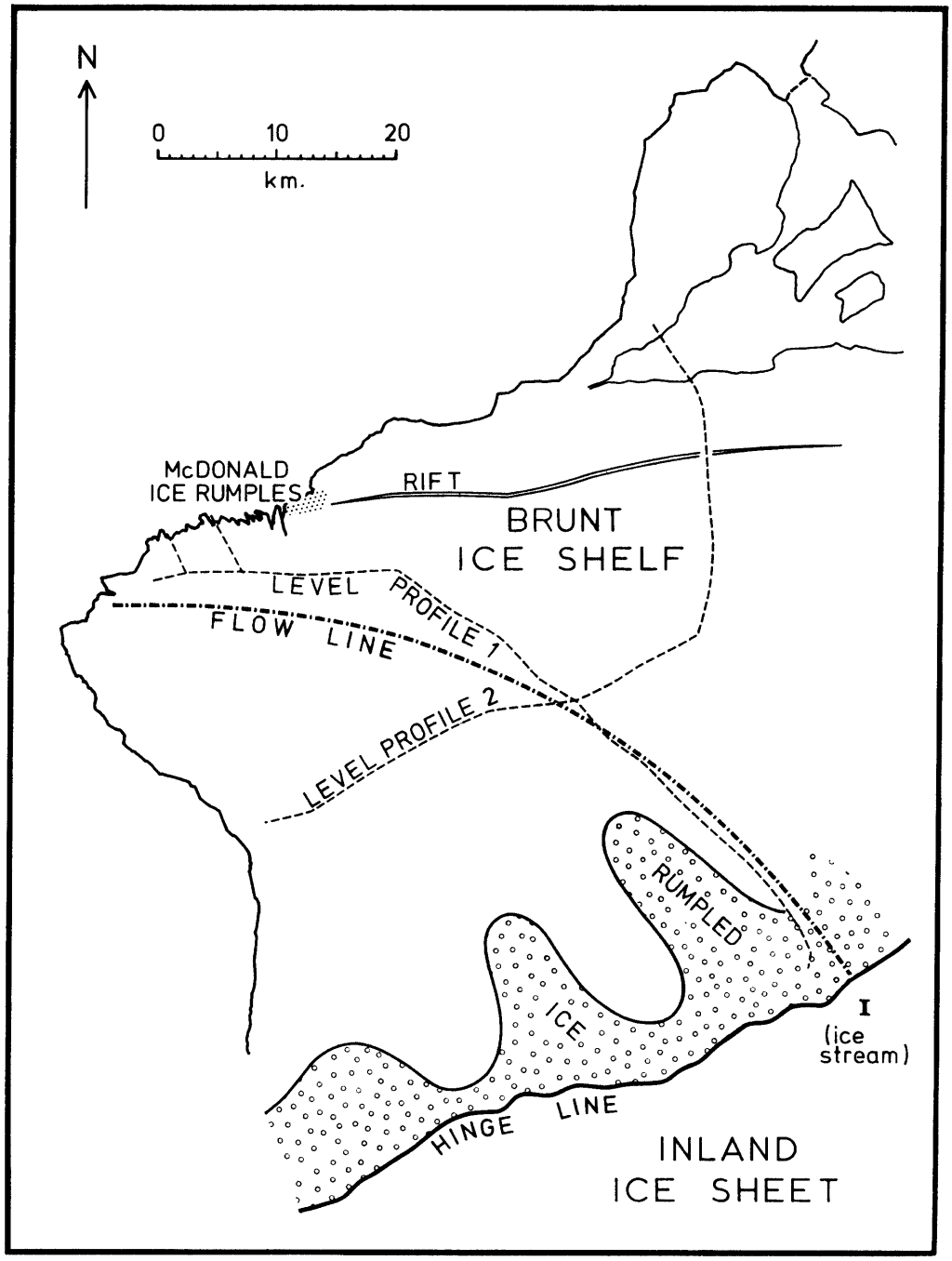

FIGURE 8

b. The western part of the Brunt Ice Shelf, showing the positions of levelling traverses and limits of rumpled ice associated with the hinge line. In September 1971 all ice to the north of the rift shown calved to form several large icebergs.

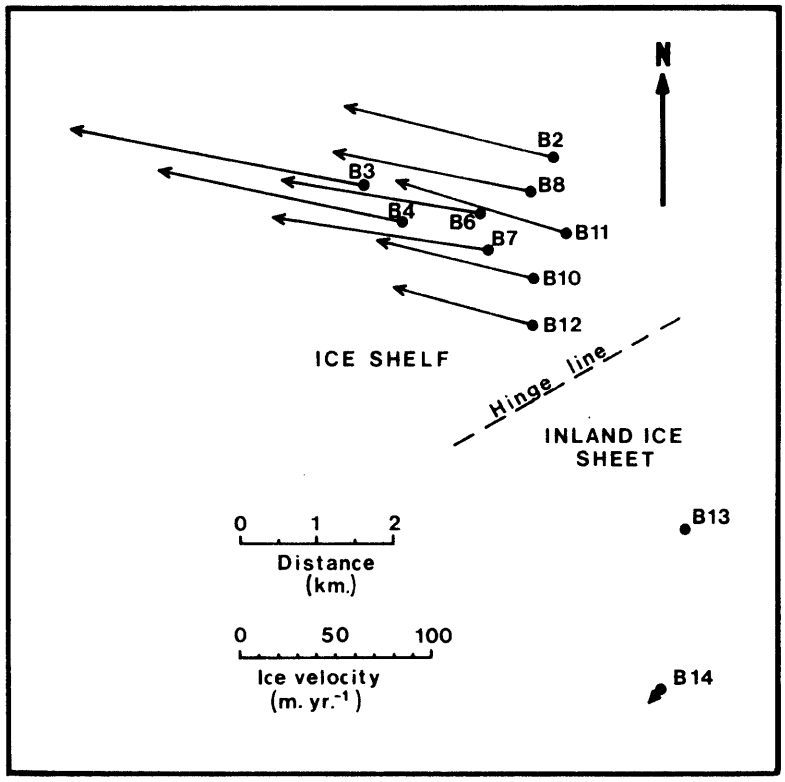

FIGURE 9

Relative ice movement near the hinge line with stake B13 as origin. The scheme was situated between stakes 63 and 64 (Fig. 5).

a regional down-slope strain-rate of 2×10^{-3} yr.$^{-1}$, the ice velocity at stake 64 was extrapolated to the probable value at stake B13, 9 km. down-slope from stake 64, which was then used to convert the relative ice velocities of the "B" scheme to absolute values. A selection of these is included in Fig. 6a.

b. *Growth rate of thin ice shelf.* A second small survey scheme was positioned near R7 (Figs. 7 and 10). Using the method described above, relative velocities were calculated for each of the survey stakes and, by comparing repeated astro-fixes, these were transformed to absolute velocities (Fig. 11).

C. DISCUSSION

Here the morphology of the ice shelf is considered in the light of the observations described. Three distinct zones can be identified and they are shown in Fig. 7.

1. *Zone 1: rapidly moving ice shelf in the north*

The most active part of the ice shelf is the northern zone where the ice front is advancing more than 1 km. each year. This rapid movement is caused by the "Dalgliesh Ice Stream" which represents the source of most of the ice in this area and which, at its point of entry into the ice shelf, is formed from two ice streams draining the areas to the north and south of Heimefrontfjella. The southernmost of these appears to be the main tributary and its direction coincides with that of the line of disturbance extending into the ice shelf. Where it becomes afloat, the surface of the ice stream (Plate I) is seen to be chaotic and is reminiscent of the floating lower reaches of Byrd Glacier (Swithinbank, 1963). In both cases, thick rapidly moving glaciers enter ice shelves and become intensely disturbed at the point of flotation where the basal shear stress decreases suddenly to zero and where there is a correspondingly rapid increase in horizontal strain.

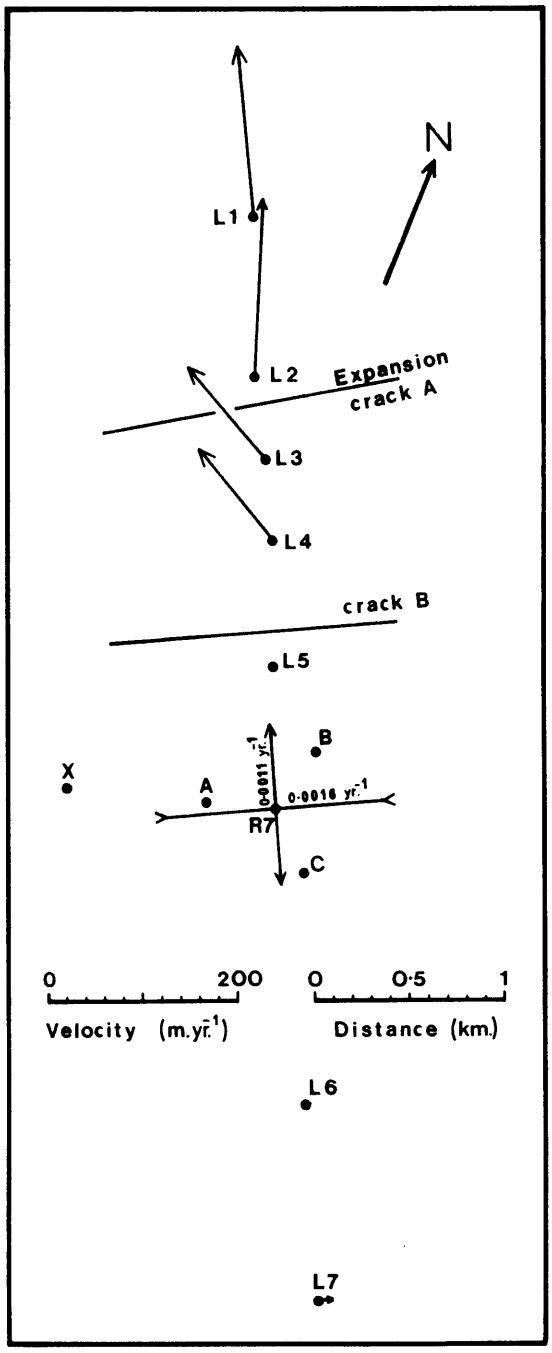

FIGURE 10a

Relative ice movement with R7 as origin and principal strain-rates at R7.

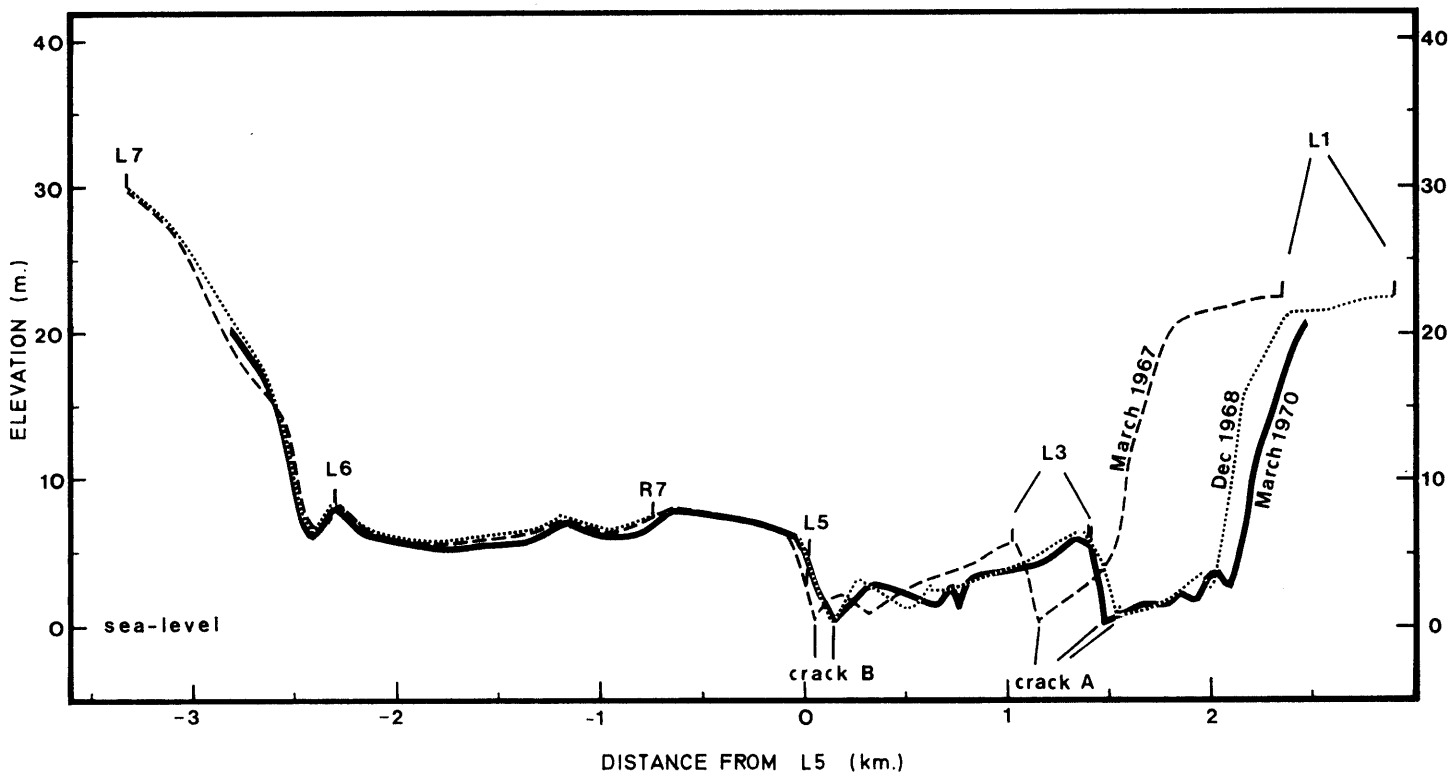

FIGURE 10b

The thin ice shelf. Despite small differences in the levelling routes, the surface-elevation profiles clearly illustrate the steady growth in area of the thin ice shelf.

a. *Strain-rates at the hinge line.* On the grounds of conservation of mass, it can be shown (Paterson, 1969, p. 101) that the longitudinal strain-rate $\dot{\epsilon}_x$ for a steady-state glacier of thickness H, surface slope α, surface velocity u and net mass balance expressed as a vertical thickness of ice b is:

$$\dot{\epsilon}_x = \frac{b + u \tan \alpha}{H} \tag{5}$$

provided that bottom melting, transverse strain-rate, and bottom sliding or bottom slope are assumed to be negligible. Positive values for any of these would tend to decrease $\dot{\epsilon}_x$. For Byrd Glacier, $b \sim 0{\cdot}5$ m. yr.$^{-1}$, $u \sim 800$ m. yr.$^{-1}$, tan $\alpha \sim 0{\cdot}01$, and $H \sim 1{,}000$ m., so a maximum value of

$$\dot{\epsilon}_x \sim \frac{0{\cdot}5 + 8}{1{,}000} \sim 1 \times 10^{-2} \text{ yr.}^{-1}. \tag{6}$$

For an unconfined ice shelf, Weertman (1957) showed that the strain-rate is proportional to the nth power of the thickness, where n is the ice flow-law exponent. At unconfined points on the Brunt Ice Shelf where ice thickness is 250 m. the strain-rate is approximately $1{\cdot}5 \times 10^{-3}$ yr.$^{-1}$, so assuming $n = 3$ the "Weertman" strain-rate for a 1,000 m. thick ice shelf is about 1×10^{-1} yr.$^{-1}$. Thus, when the glacier becomes afloat, the strain-rate increases by at least an order of magnitude with a corresponding increase in the intensity of crevassing.

It has been assumed here that at the hinge line the floating ice is relatively unconfined. Whilst this is so in the case of the Brunt Ice Shelf, Byrd Glacier enters a confined area of the Ross Ice Shelf. However, it becomes afloat in a channel between rock walls that diverge sufficiently to permit transverse strain at the rate of about 2×10^{-2} yr.$^{-1}$. This probably explains why the lines of fracture in Byrd Glacier trend parallel with the direction of flow. If the ice is moving rapidly seaward, the resultant tongue of

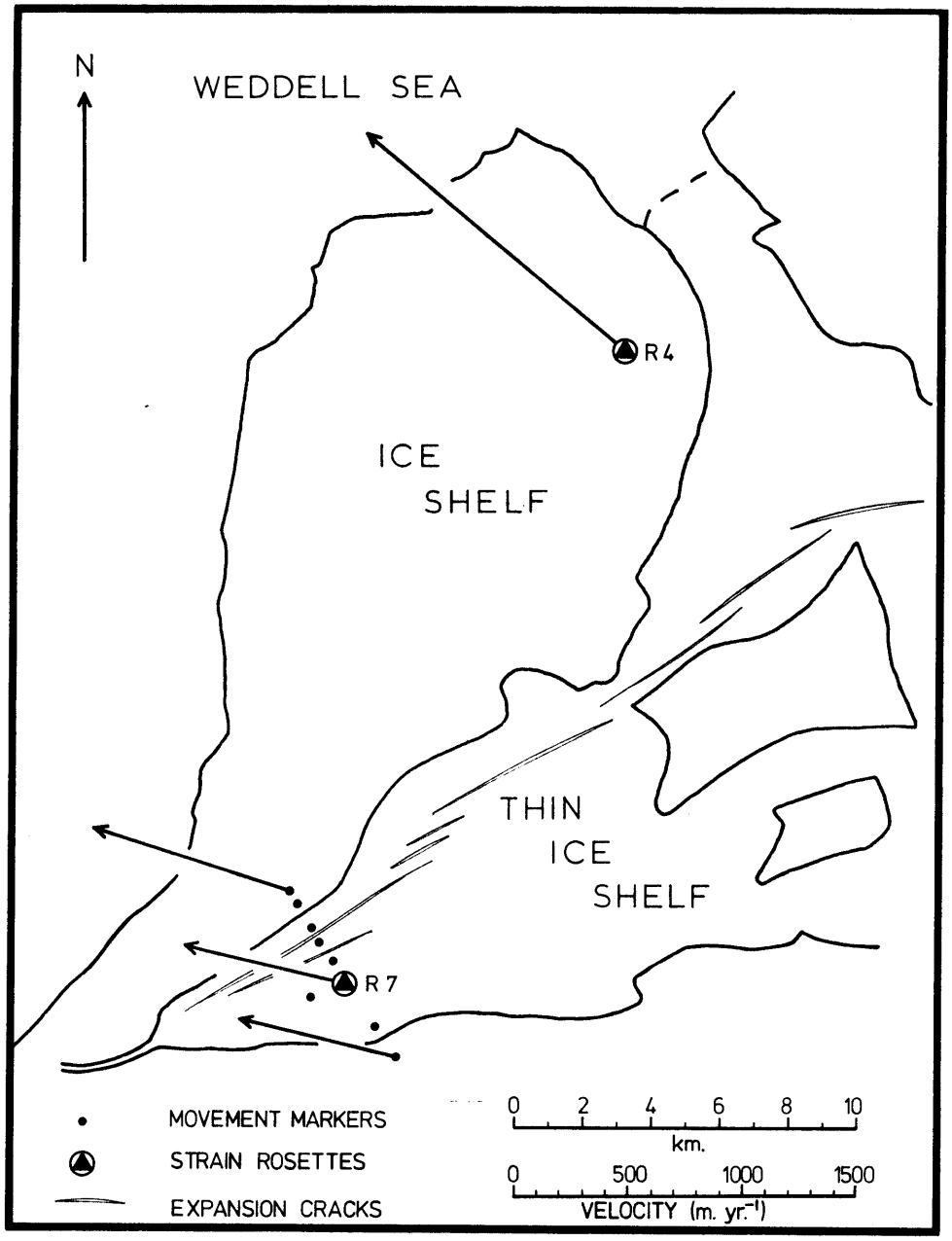

FIGURE 11

The thin ice shelf. The large slab of ice shelf to the north of R7 is pivoting about its "neck", causing rapid growth in area of the thin ice shelf.

disturbance will persist for a considerable distance into the ice shelf. From Weertman (1957), the vertical strain-rate

$$\dot{\epsilon}_z = -k(H)^n, \tag{7}$$

where k is a constant which depends on temperature and on the ratio of the two principal components of the horizontal strain-rate. Assuming that $n = 3$, Equation (7) can be re-written

$$\frac{dH}{H^4} = -k\,dT. \tag{8}$$

It can also be assumed that k is independent of position within the disturbed "tongue". Then, on integration, Equation (8) becomes:

$$\frac{1}{H_2^3} - \frac{1}{H_1^3} = 3k(T_2 - T_1) = 3k\Delta T. \tag{9}$$

By putting H_1 equal to ice thickness at the hinge line and H_2 equal to that where crevasses no longer form, ΔT is the time for ice to pass between these points. H_2 is ice thickness where the largest tensile horizontal strain-rate equals the critical value ($\dot{\epsilon}_c$) for crevasse formation, and $\dot{\epsilon}_z$ = −(sum of longitudinal and transverse strain-rates) = $r\dot{\epsilon}_c$. For a completely unconfined ice shelf $r = -2$ and for one free to creep in only one direction $r = -1$.

For an ice stream becoming afloat H_2^3 is usually $<<H_1^3$ and from Equation (7)

$$H_2^3 = \frac{-\dot{\epsilon}_z}{k} = \frac{-r\dot{\epsilon}_c}{k}, \tag{10}$$

so Equation (9) becomes:

$$\Delta T \sim -\frac{1}{3r\dot{\epsilon}_c}. \tag{11}$$

In arriving at this relatively simple result, the effects of both surface accumulation and bottom melting have been neglected, but these are unlikely to be significant as long as their combined effect on ice thickness is appreciably less than $|rH_2\dot{\epsilon}_c|$.

For the Brunt Ice Shelf $\dot{\epsilon}_c \sim 6 \times 10^{-3}$ yr.$^{-1}$, and at *R*5 $r \sim -1{\cdot}5$, giving $\Delta T \sim 36$ yr. The average forward velocity over this period is about 1 km. yr.$^{-1}$, so active crevassing should extend 30–40 km. into the ice shelf. Thereafter, it may take between 10 and 20 yr. for drift-snow accumulation to smooth the ice-shelf surface, and the total length of the tongue of disturbed ice becomes 40–60 km., which is in good agreement with the observed 50–70 km. For the Byrd Glacier "tongue", r probably equals −1 and active crevassing is observed 80–100 km. beyond the line of flotation (personal communication from C. W. M. Swithinbank). Assuming an average forward velocity of 1 km. yr.$^{-1}$ and substituting these values in Equation (11) gives $\dot{\epsilon}_c \sim 3 \rightarrow 4 \times 10^{-3}$ yr.$^{-1}$, which is close to Holdsworth's (1969*a*) value for a 10 m. temperature of −28° C.

The surface crevassing at flotation is probably accompanied by the opening of crevasses from beneath. Evidence for the existence of such crevasses is supplied by observations from two sources. Kehle (1964, p. 261) concluded that sea-water in crevasses which terminated at least 1 km. from the nearest open sea must have entered from below, "implying that the crevasses must extend to the bottom of the shelf even though extrapolation of their rate of closure with depth suggests that they terminate above the bottom". Near-surface radio echoes from within the Ross Ice Shelf from features similar to but narrower than those described by Harrison (1970, p. 1103) have been interpreted by Harrison (personal communication) as bottom crevasses.

Weertman (1969) calculated the penetration "depth" of isolated bottom crevasses formed in a freely floating ice sheet as $\pi H/4$. Because the bottom temperature is that of the underlying sea-water, the critical strain-rate for crevasse formation will be larger than at the surface ($1 \rightarrow 3 \times 10^{-2}$ yr.$^{-1}$ compared with 6×10^{-3} yr.$^{-1}$). This means that bottom crevasses, if they form, will be less closely spaced than those at the surface. If the spacing is greater than the ice thickness, the penetration "depth" will be approximately $\pi H/4$. Rifts penetrating the ice sheet from top to bottom have been observed on ice shelves in areas where there is probably local thinning near the hinge line; these may have been caused by linking of bottom and top crevasses.

b. *Calving at the ice front.* Some ice shelves calve intermittently to produce giant icebergs (Ledenev and Yevdokimov, 1965; Budd, 1966, p. 355), while between these events the ice front advances far beyond the equilibrium configuration defined by the positions of grounded ice. Indeed, the present observations on the Brunt Ice Shelf appear to indicate that calving of small icebergs is seldom sufficiently regular to keep pace with a rapidly advancing ice front. Fig. 7 shows three plots of the Brunt ice front from 1915 (F. Worsley, unpublished track chart of *Endurance*), 1955 (track chart of the icebreaker *General San Martín*) and 1968 (chart compiled by A. Johnston from surface observations on the ice shelf and radar plots made from M.V. *Kista Dan* and R.R.S. *John Biscoe*). The position of the ice front near points of grounding is

almost identical in each plot, but between 1955 and 1968 the ice front in zone 1 advanced about 10–15 km., a distance in reasonable agreement with that derived from the velocity measured at R5 (1·3 km. yr.$^{-1}$). On each side of this rapidly advancing ice front the ice fractured to form a series of parallel rifts aligned perpendicular to the direction of maximum strain. At some time between 1915 and 1955 large-scale calving removed the promontory of freely floating ice marked in Fig. 7 as the "Stancomb-Wills Promontory". Possible calving mechanisms will be reviewed on p. 26.

2. *Zone 2*

Between the rapidly moving ice of zone 1 and the slower ice of zone 3 the ice shelf suffers intense shearing. Rifts penetrate right through the ice shelf and large slabs are dragged out of the ice shelf immediately to the south of the shear zone (zone 2 in Fig. 7). Sea ice formed between the rapidly separating slabs is protected from erosion by the surrounding ice shelf. Under these conditions the sea ice rapidly thickens both by the freezing of sea-water and also by the accumulation of drift snow to form thin ice shelf. However, its thickness seldom exceeds 50 m., and its boundaries are clearly defined by ramped cliffs leading up to the older ice shelf (Plate IIa).

The most rapidly moving slab of ice shelf is that nearest to the ice front. Strain rosette R4 was situated near its northern tip and R7 on the thin ice shelf to the south, together with a triangulation network along a line linking adjacent pieces of thicker ice shelf (Figs. 10 and 11). R4 was found to be moving north-west at 1·5 km. yr.$^{-1}$, a velocity which is approximately equal to that of the ice front in zone 1. The ice-shelf section is pivoting in an anti-clockwise sense about the narrow neck of ice linking it to the rest of the ice shelf. Consequently, the thin ice shelf to the south is increasing in area.

A series of surface profiles obtained at different times across the same section of the thin ice shelf is shown in Fig. 10. The growth in area of the thin ice shelf is well illustrated, even at the scale of the diagram, by the increasing distance between ice ramps leading to thicker ice shelf. Growth takes place in a series of expansion cracks which extend parallel with the south bank of the pivoting section. In order to detect short-period fluctuations in growth rate, frequent measurements were made between markers planted on each side of cracks A and B. These are plotted against time in Fig. 12. The mean rate of opening was 0·18 m. day^{-1} (66 m. yr.$^{-1}$) at crack A and 0·1 m. day^{-1} (37 m. yr.$^{-1}$) at crack B. Superimposed

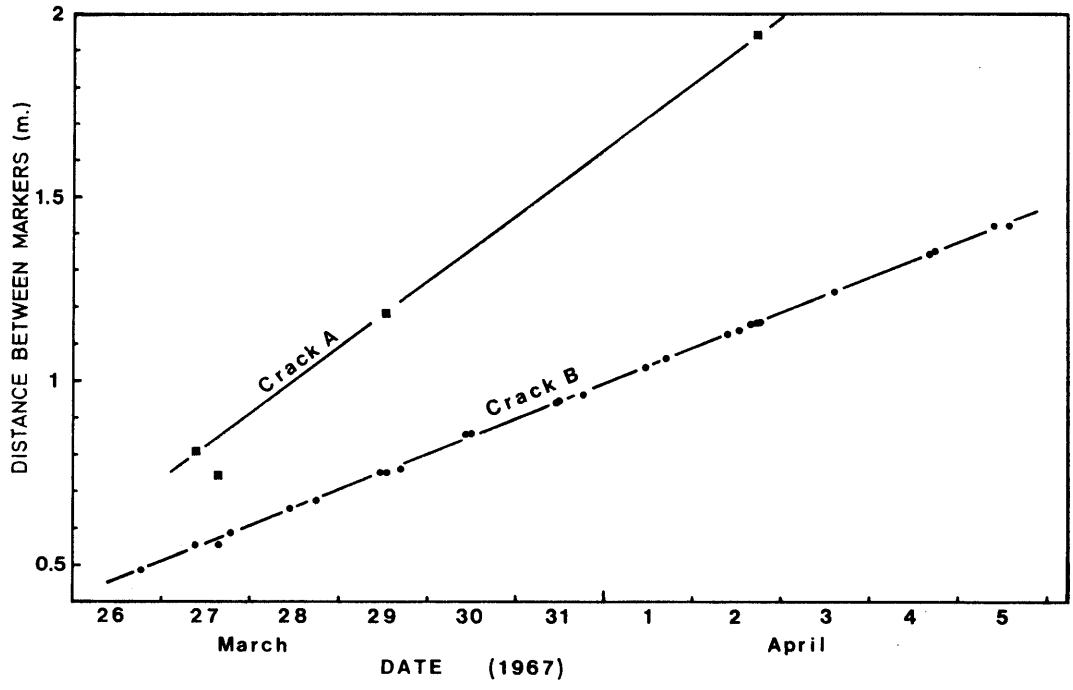

FIGURE 12

The distance between markers on each side of expansion cracks in the thin ice shelf plotted against time. See Fig. 10 for the positions of cracks.

on the mean values was an apparently cyclic variation with a period of about 1 day, but measurements were not sufficiently regular to indicate whether or not this was due to tidal effects.

In a hole drilled near the centre of R7 liquid brine was found at a depth of 8·7 m., which was 1·5 m. below sea-level. Its temperature was −10° C, corresponding to a salinity of approximately 125 °/₀₀. Immediately below the brine layer was bubbly impermeable ice. Stuart and Bull (1963) suggested that the brine layers in the Ross Ice Shelf were due to vertical infiltration of brine through the lower layers of the ice shelf. This may take place near the ice front where bottom melting has exposed permeable firn, but Hochstein and Risk (1967) found brine layers underlain by impermeable ice and postulated horizontal seepage as the cause. The brine layers in the Brunt Ice Shelf are believed to have originated in this way.

3. *Zone 3*

Movement of the southern part of the ice shelf (zone 3) is hindered by grounded ice on the McDonald Ice Rumples. However, the movement pattern is dominated by the "Dalgliesh Ice Stream" which causes the ice of zone 3 to pivot about its south-west corner. The pivoting is illustrated by the ice-velocity vectors shown in Fig. 6a. Apart from measurements near the McDonald Ice Rumples, there is an approximately linear increase in velocity with increasing distance from the south-west corner of the ice shelf. Consequently, along most of the hinge line the velocity of the ice shelf is considerably greater than that of the land ice, which calves to form icebergs separated by expanses of sea ice (Plate IIb). Similar features were observed on the Riiser-Larsenisen by Swithinbank (1957*a*), who noticed the constant distance between successive icebergs and suggested that they were separated by the forces exerted when seawater froze in tide cracks. Because tidal movement can only take place immediately along the hinge line, active separation is confined to this area and hence to the time interval between successive calvings. However, the forces involved are relatively small and are unlikely to be responsible for the seaward motion of the entire ice shelf as implied by Swithinbank (1957*a*, p. 27). Instead, it is believed that iceberg formation can only take place where a state of tension exists across the hinge line. Such conditions often occur between the points of entry of rapidly moving ice streams which push the ice shelf *en masse* seaward. The size of icebergs formed at a fixed point is remarkably constant and on p. 30 it is suggested that they calve when the bending stresses induced at flotation equal the fracture strength of ice.

The separation S between icebergs is determined by the strain-rate across the hinge line, and on the Brunt Ice Shelf it is expected that this would be approximately proportional to the distance from the point about which zone 3 is pivoting. S and the iceberg width perpendicular to the hinge line (W in Fig. 13) can be estimated from air photographs. Assuming steady-state, the time T between successive calvings at any fixed point is:

$$T = W/V_1 = S/V_2. \tag{12}$$

$$\text{So } V_2 = V_1 S/W, \tag{12a}$$

where V is the component of velocity perpendicular to the hinge line and subscripts 1 and 2 refer to grounded and floating ice, respectively. In Table II measurements of V_1 and estimates of S/W from air photographs are used to calculate values of V_2 at three points along the hinge line. These show good agreement with the results of the ice-movement survey.

Rapid accumulation of drift snow fills in the gaps between adjacent icebergs, and 20 km. from the hinge line along the triangulation net they have become little more than gentle undulations in the surface, in marked contrast to the large expanses of thin ice shelf in zone 2. The difference is probably explained by the smaller spacing of icebergs near the hinge line in zone 3 and the consequently larger drift-snow accumulation in the gaps between them. Furthermore, water circulation between closely spaced icebergs is minimal and conditions favour thickening of the sea ice by bottom freezing.

Assuming the ice shelf to be approximately in hydrostatic equilibrium across these undulations, and knowing the surface velocity, the mean rate of thickening of new ice shelf can be estimated to be approximately 3 m. yr.$^{-1}$ during the first 60 yr. of its existence. Although excessive snow-drift accumulation is at least of this order between the icebergs close to the hinge line, it rapidly decreases farther north where the surface profile becomes smoother. If the ice is not in hydrostatic equilibrium across the undulations, the rate of thickening of new ice shelf may be considerably less, the new ice shelf being supported by the surrounding icebergs in the same way that a snow bridge is supported by the firm ice on each side of

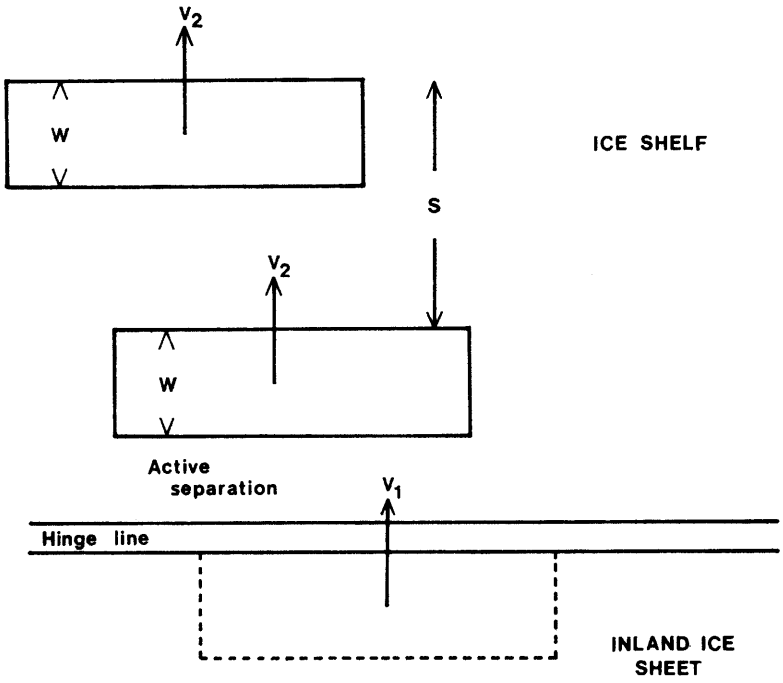

FIGURE 13
Iceberg separation at the hinge line.

TABLE II
ICE-SHELF VELOCITIES DEDUCED FROM OBSERVED ICEBERG SEPARATION AT THE HINGE LINE

	East side of stake line	*West side of stake line*	*Near R3*
V_1 (m. yr.$^{-1}$)	170	70	65
S/W	2±0·5	4±0·5	1·6±0·3
$V_2=\frac{V_1 S}{W}$ (m. yr.$^{-1}$)	340±85	280±35	104±20
V_2 from movement survey (m. yr.$^{-1}$)	310	280	115

a crevasse. It follows that ice in the valleys would be slowly sagging in relation to that of the adjacent ridges. There was, however, no evidence for this in repeated levelling profiles. Unfortunately, ice thicknesses from radio echo-sounding in such areas are unreliable because much of the new ice shelf is permeated with sea-water and radio waves are unable to penetrate to the bottom surface.

Where small ice streams enter the ice shelf, the increase in velocity across the hinge line is not so pronounced, and the relatively narrow rifts between icebergs are more rapidly smoothed by drift-snow accumulation than they are where the gaps are wider. This is clearly seen in Plate IIb where the ice stream at point I leads to a relatively smooth ribbon of ice shelf along which the eastern limb of the stake network (Fig. 8b) was planted. Where air photographs are available such features can be used to map flow lines.

The McDonald Ice Rumples. The effect on ice flow of the grounded area in the north-west of zone 3 is seen in Plate III. The pressure waves from which the McDonald Ice Rumples get their name lie up-

stream of the grounded ice, and large crevasses have opened across the crests of these waves. Kehle (1964) attempted to interpret similar features on the Ross Ice Shelf near "Camp Michigan" using Biot's (1959) analysis of folding. Kehle's model involves some buckling of the lower layers of the ice shelf and the predicted wave-lengths are not in good agreement with those observed. Holdsworth (1970) proposed that the geometry of the waves is initially determined by surface instability resulting from inhomogeneities in the ice, and he was able to predict wave-lengths in good agreement with those observed in the Ross Ice Shelf near McMurdo Sound.

Thomas (1973*b*) used strain-rates measured near the McDonald Ice Rumples to examine the effects on the ice shelf of the area of grounded ice. The average stress acting across the boundary between grounded and floating ice was calculated to be about $1{\cdot}7 \times 10^6$ N m.$^{-2}$, at least an order of magnitude greater than that necessary for crevasse formation. Plate III illustrates the effects of these very large stresses on the ice shelf at the point of grounding. The effects of the very large transverse stresses up-stream from the grounded ice were highlighted in December 1968. The year before, a new line of crevasses had been observed extending east from the McDonald Ice Rumples for about 4 km; they can hardly be seen in Plate IIIa. The situation was virtually unchanged in early December 1968 but by the middle of the month the crevasses had joined to form one 5 km. long crack that terminated abruptly up-stream of the grounded ice. Over most of its length the crack was less than 1 m. wide. 10 days later it had widened slightly and extended a further 9 km. to the east. It continued to extend but at a diminishing rate, while at the same time rapidly widening so that when air photographs were again taken in January 1970 the crack had become a rift 100 m. wide (Plate IIIb) floored with sea ice and open sea-water. Its position in April 1970 is shown in Fig. 8b.

Similar rifts have been reported on other ice shelves (Wilson, 1960; Fleet, 1965) and they can usually be explained by differential movement due either to local grounding or to the influences of nearby ice streams. In its early stages, a rift can be considered to open elastically, with the result that the tensile stresses across the ends become so large that the rift rapidly extends. This corresponds to the initial stage observed in the development of the rift on the Brunt Ice Shelf, when rapid longitudinal extension was accompanied by negligible opening. As the rift increased in length, stresses were relieved more by creep bending of the ice on each side than by elastic bending. This resulted in a reduced rate of growth and a rapid increase in the rate of opening. Because the rift terminated at the grounded ice of the McDonald Ice Rumples, it was at first unable to reach the ice front. The rift continued to widen to form an area of thin ice shelf bounded seaward by thicker ice pivoting about the grounded ice. However, in September 1971 the segment of thicker ice calved taking with it a large area of thin ice shelf including R7 and the segment of ice shelf where R4 was planted (Figs. 2 and 8b). Rifts probably form periodically in about the same position up-stream of the grounded ice when the transverse stresses reach some critical value. In this way, long and relatively narrow icebergs are intermittently calved from the ice shelf.

The formation of such a rift evidently relieves the stresses up-stream from the McDonald Ice Rumples, so that ice to the south of the rift is able to slide more rapidly past the grounded ice. This is seen in Fig. 14, where measurements of relative velocity between the grounded ice and Halley Bay station are

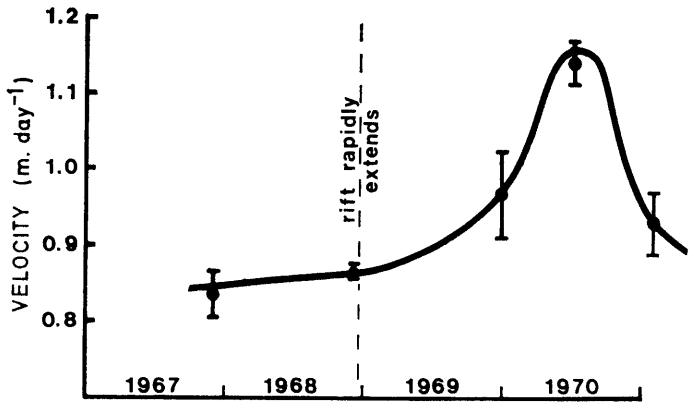

FIGURE 14

Relative velocity of Halley Bay station with respect to a beacon on the McDonald Ice Rumples.

plotted against time. At approximately the time when the rift was first observed the ice shelf near Halley Bay began to accelerate rapidly and, farther south, strain-rates measured at R8 recorded a sudden increase in the component of shearing in an east–west direction. This continued until, as a result of ice movement, the rift was shifted sufficiently to the north to allow piling of ice once more against the grounded ice and a corresponding reduction in ice velocity at Halley Bay.

III. THE CALVING OF ICEBERGS

A. Existing Theories

Reeh (1968) considered the stress field due to the bending moment at an ice front and suggested that a floating glacier is warped downwards as shown in Fig. 15, where u is the vertical deflection of any

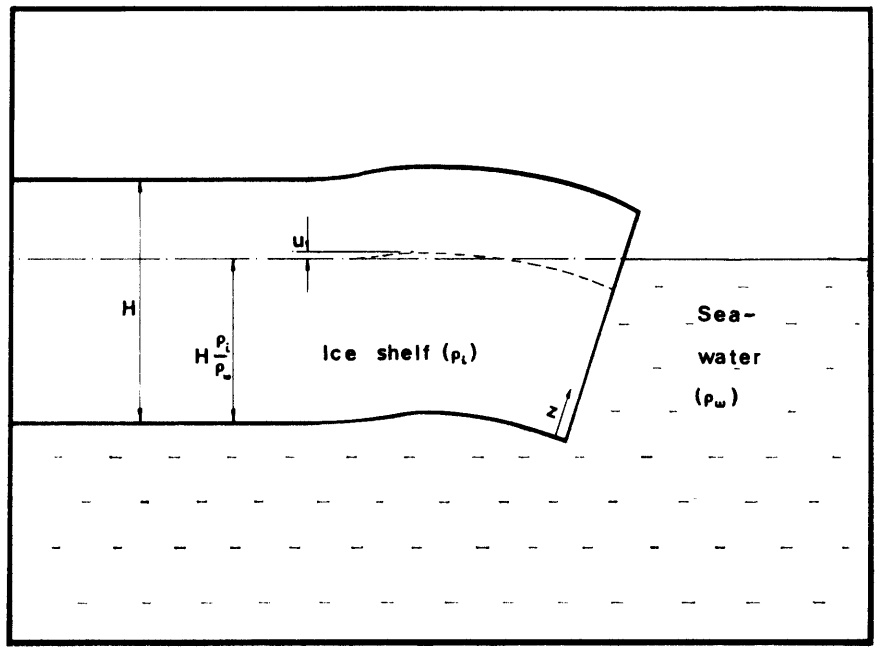

Figure 15

Longitudinal section of an ice shelf near the ice front.

point in the glacier from its undisturbed state. Reeh showed that at the ice front the magnitude of the bending moment increases as the ice becomes more submerged. This leads to continued warping, and near the ice front the shear stress in the vertical plane perpendicular to the ice front increases with time. It reaches a maximum at a distance from the ice front equal approximately to half the ice-shelf thickness. For an ice shelf of 200 m. thickness, mean density 850 kg. m.$^{-3}$ and mean temperature $-12°$ C, Reeh's model predicts that, after a calving event, it would take about 50 yr. for the maximum shear stress to reach the relatively low value of 3×10^4 N m.$^{-2}$. At about the same distance from the ice front the longitudinal tensile stress at the upper surface also reaches a maximum ($\hat{\sigma}_{xx}$) which is almost independent of time and is about 50 per cent greater than the equilibrium value at large distances from the ice front. For the example quoted above $\hat{\sigma}_{xx} \sim 1{\cdot}5 \times 10^5$ N m.$^{-2}$ which, according to Meier (1958, p. 506), is sufficient to initiate fracture if the stress is sustained.

Since Reeh assumed the viscosity of ice to be independent of temperature and stress, some of his quantitative results are unlikely to represent the situation in an actual ice shelf. However, the value of $\hat{\sigma}_{xx}$ is hardly affected by this simplification and, if fracture is caused by the high value of $\hat{\sigma}_{xx}$ near the ice front, the time interval between calving is probably determined by the time dependence of fracture in terms of temperature and applied stress. At present we can only say that the time to fracture decreases

with increasing temperature or with increasing tensile stress. The distance from the ice front at which fracture takes place will be of the same order as the ice thickness.

Observations on the Brunt Ice Shelf show that many areas of ice front have survived for at least 10 yr. without calving. During the same period the ice front has advanced up to 15 km., so "Reeh" calving is unlikely to keep pace with ice-shelf movement. However, it may occur sufficiently often to account for the relatively fresh appearance of most ice fronts. The magnitude of $\hat{\sigma}_{xx}$ is roughly proportional to ice thickness and the time interval between calving events can be expected to be greatest for a thin cold ice shelf. Thus a combination of low surface accumulation and rapid bottom melting near the ice front could thin the ice shelf sufficiently to prevent "Reeh" calving ever taking place. This could account for the low, shelving ice fronts encountered by *Endurance* on the "Stancomb-Wills Promontory" (F. Worsley, unpublished track chart of *Endurance*, 1915).

The influence of tidal movement on the flexure of floating ice sheets has been investigated by Robin (1958, p. 122). Robin considered the ice shelf as a thin elastic sheet clamped along the hinge line, with the free portion able to rise and fall with the tide within the limits imposed by the elastic forces. With the assumption that at a sufficient distance from the hinge line the ice shelf rises and falls freely with the tide, Robin obtained a relationship between surface stress and distance from the hinge line. This showed that, for a 200 m. thick ice shelf with a tidal range of 1 m., the surface stresses at the hinge line reach a maximum of about 6×10^5 N m.$^{-2}$ with a second much reduced stress maximum at about 2 km. seaward away from the hinge line. This conclusion is in good agreement with the observed position of a group of strand cracks at the hinge line and a second group of cracks at between 1 and 2 km. from the hinge line on the Maudheim ice shelf.

Robin's analysis can be applied only when the seaward extent of the ice shelf is much greater than its thickness. Holdsworth (1969*b*) considered the dependence of hinge-line stresses on seaward length of floating ice. He concluded that for an ice thickness of 200 m. and tidal range of 1 m. the tensile stress across the hinge line reaches a maximum of about 1·5 MN m.$^{-2}$ when the seaward length of floating ice is between 3 and 4 km. The hinge-line stresses were found to be proportional to tidal range and this may explain why, although long floating glacier tongues such as that of Erebus Glacier were able to survive in the Ross Sea with a tidal range of 1 m., no similar tongues are found in the Weddell Sea where the maximum tidal range is perhaps three times larger (Thiel and others, 1960, p. 635).

Holdsworth (1969*b*) also presented an approximate steady-state creep analysis of tidal bending. For a 200 m. thick ice shelf, Holdsworth's equations give a surface hinge-line stress of about 1 MN m.$^{-2}$ if flow-law parameters appropriate to an ice temperature of −15° C (Thomas, 1973*b*) are adopted. Thus, both the elastic and the steady-state creep analyses predict tide-induced stresses at the hinge line which are probably large enough to fracture the relatively weak upper layers of the ice shelf, and to explain the formation of strand cracks along the hinge line. However, the existence of long floating ice tongues and ice shelves implies that the hinge-line stresses are seldom sufficient to initiate calving.

At a distance from the hinge line greater than 10 km. the Robin–Holdsworth analysis predicts negligible tide-induced stresses and the calving of giant icebergs from the ice front is unlikely to be initiated by tidal movement.

B. Influence of Tsunamis on Large Ice Tongues

Tsunamis have been invoked as a possible source of the energy necessary to initiate calving (Swithinbank and Zumberge, 1965, p. 211; Loewe, 1969, p. 322). If it is assumed that the effect of a tsunami passing beneath the ice front is to bend the ice shelf into a wave form, a relationship between wave amplitude and wave-length for calving to take place can be deduced. Rectangular axes are used with the x-axis at sea-level and positive towards the ice front, and z is positive upwards. It is assumed that the ice shelf behaves as an elastic sheet with areal dimensions large compared with its thickness. If it adopts a wave of the form $z = a \sin(2\pi x/\lambda)$ with a the amplitude and λ the wave-length, the bending stress at the surface of the ice shelf is:

$$\sigma_x = -\frac{EH}{2(1-\nu^2)} \cdot \frac{\mathrm{d}^2 z}{\mathrm{d}x^2} = \frac{2EHa\pi^2}{\lambda^2(1-\nu^2)} \sin(2\pi x/\lambda), \tag{13}$$

where E is Young's modulus in bending $\sim 3 \times 10^9$ N m.$^{-2}$, H is the ice thickness and ν is Poisson's ratio $\sim 0{\cdot}3$ (values of E and ν from Dorsey (1940, p. 445)). Putting $H = 200$ m., the maximum bending stress is:

$$\hat{\sigma}_x \sim 1{\cdot}3 \times 10^{13} (a/\lambda^2) \text{ N m.}^{-2}. \quad (14)$$

Holdsworth (1969*b*) estimated that floating glacier tongues in the Ross Sea must have survived rapidly applied tensile stresses of the order of $1{\cdot}5$ MN m.$^{-2}$ without calving, so $\hat{\sigma}_x$ must exceed this figure for calving to be triggered by tsunami-induced stresses alone. This leads to the condition:

$$a/\lambda^2 > 1{\cdot}1 \times 10^{-7} \text{ m.}^{-1}. \quad (15)$$

In order to calculate the equivalent ratio (a_t/λ_t^2) for the tsunami, values of a_t and λ_t over the continental shelf are needed. Tsunami wave-lengths are large compared with sea depth (d) and the wave velocity (V) can be expressed by the equation: $V = (gd)^{\frac{1}{2}}$, where g is the acceleration due to gravity, and for constant period λ_t is proportional to $d^{\frac{1}{2}}$. On grounds of conservation of energy, it can be shown (Defant, 1961, p. 21) that $a_t^2 V$ is constant if dissipative mechanisms are neglected, so a_t is proportional to $d^{-1/4}$ and a_t/λ_t^2 is proportional to $d^{-5/4}$. Values of a_t and λ_t for a tsunami in the open ocean have not been measured but, assuming measurements made on Wake Island (Wiegel, 1964, p. 100) in the western Pacific Ocean to be typical of a sea depth of 4,000 m., values for the 4 November 1952 Kamchatka tsunami are: $a_t \sim 0{\cdot}3$ m., $\lambda_t \sim 100$ km., and $a_t/\lambda_t^2 \sim 3 \times 10^{-11}$ m.$^{-1}$. If d is suddenly reduced to about 200 m. at the continental slope, a_t/λ_t^2 becomes $1{\cdot}3 \times 10^{-9}$ m.$^{-1}$, which is about 1 per cent of the value in Equation (15) and this is further reduced if energy is lost either by reflection at the continental slope or by passage of the wave through the relatively shallow water above the continental shelf. However, little is known about the interaction between floating bodies and waves, and the combined effects of a shelving sea bed beneath the floating ice and of the ice shelf itself may modify the tsunami in such a way that large stresses are induced in the ice shelf at some distance back from the ice front.

Seiche-like oscillations might also be expected to occur beneath the ice shelf if the period of the tsunami coincides with the natural period of the ice shelf. Reeh (1970) suggested that a similar phenomenon may have been responsible for violent periodic oscillations of water level in the bay of Jakobshavn. In his paper, Reeh derived an expression for the natural period of a floating rectangular ice sheet, anchored along the hinge line and supported at its sides, in terms of its dimensions and the water depth beneath the ice sheet. Assuming that the behaviour of a large ice tongue approximates to that of an infinitely wide floating ice sheet, extrapolation of Reeh's fig. 5 can be used to give a rough estimate of natural period T. For a 200 m. thick ice tongue 100 km. square with a bottom clearance of 200 m., $T \sim 150$ min. and this is roughly proportional to seaward length. This figure represents an upper limit since the finite width of the ice tongue implies a reduction in T. Thus the natural period of the fundamental vibration, or of one of the harmonics, may fall within the range of observed tsunami periods (10–30 min.). Then a given tsunami might be expected to trigger calving in only those ice tongues with the appropriate dimensions. Frequent mapping of the Antarctic coastline by satellite photography should reveal any correlation between calving events and the occurrence of tsunamis.

C. Effects of Sea Currents on Floating Ice Tongues

Wilson (1960) suggested that the "great ice chasm" in the Filchner Ice Shelf was caused by the frictional drag of strong sea currents. To obtain a rough estimate of the shear stress across the chasm due to viscous drag on the underside of the seaward arm of the ice shelf the equations used by Campbell (1965, p. 3285) in calculating the frictional drag of sea currents on ice floes in the Arctic Ocean can be applied. Solutions to these equations are critically dependent on the thickness of the boundary layer and on the bottom roughness. Here, examples from Campbell's range of possible values for these parameters have been chosen, so that the calculated stress represents a maximum probable value. Then for an ice thickness of 300 m. and sea current of 1 m. sec.$^{-1}$, the average shear stress across the chasm is about 10^3 N m.$^{-2}$. This is at least two orders of magnitude too low to cause the extensive fracture associated with the "great ice chasm". For an exposed ice tongue, however, a significant momentum transfer at the up-stream ice cliff with an associated tensile bending stress along this ice cliff might be expected. For a rectangular ice tongue of seaward length L, width D and thickness H (Fig. 16), rectangular axes are taken with the x-axis along the centre line and with the origin so that the ice front is at $x = L$. Only the component of

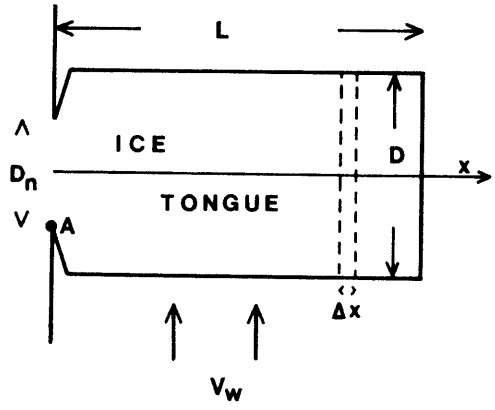

FIGURE 16
Plan view of a floating ice tongue.

water current in the positive y direction (V_w) is considered and it is assumed to be independent of position. ρ_i is the mean density of the ice shelf. It is assumed that all momentum possessed by water particles travelling towards the ice tongue is transferred to the ice. This rather severe assumption leads to an overestimation of the bending stress.

For a small vertical element of unit width, the force acting in the positive y direction equals the momentum lost per second by the sea:

$$F = V_w^2 \rho_w \left(H\frac{\rho_i}{\rho_w}\right) = V_w^2 H \rho_i. \tag{16}$$

The total moment about a vertical axis through the origin is:

$$M = FL^2/2 \tag{17}$$

and from bending theory the tensile stress at A in Fig. 16 is:

$$\sigma_x = 6M/(D_n^2 H) \tag{18}$$

where D_n is the width of the ice tongue at the point it leaves its protective margins.

With $\rho_i \sim 850$ kg. m.$^{-3}$,

$$\sigma_x \sim 2{\cdot}5 \times 10^3 L^2 V_w^2/D_n^2 \text{ N m.}^{-2}. \tag{19}$$

V_w is approximately equal to the ocean current averaged over the ice-shelf depth, which should equal the velocity of drifting icebergs. The results of frequent mapping of icebergs near Halley Bay on the Brunt Ice Shelf indicate that their average velocity is between 0·5 and 1 m. sec.$^{-1}$. The ratio (length/width) for the "Stancomb-Wills Promontory" on the Brunt Ice Shelf in 1915 (F. Worsley, unpublished track chart of *Endurance*) and for Trolltunga shortly before it calved (Anonymous, 1969, p. 62) was approximately 2. However, at the point where an ice tongue leaves its protective margins, rifts commonly penetrate several kilometres into the ice shelf so that $L/D_n \sim 4$, giving $\sigma_x \sim 2{,}500 \rightarrow 10{,}000$ N m.$^{-2}$, which is less than 10 per cent of the horizontal tensile stress due to the weight of ice above sea-level, shown by Weertman (1957) to be:

$$\sigma_t = \tfrac{1}{2}\rho_i g H(\rho_w - \rho_i)/\rho_w. \tag{20}$$

However, for sufficiently large values of (L/D_n), the combined effects of σ_x, σ_t and current drag on the ice bottom may be sufficient to cause complete fracture of the ice shelf at A.

D. HINGE-LINE CALVING

Where Beardmore Glacier becomes afloat a series of rifts stretches seaward. They appear to be faults with a downthrow of about 30 m. on the seaward side. They are spaced at regular intervals of about 1 km. and they are each about 1 km. in length and aligned parallel to the hinge line. Collins and Swithinbank (1968) suggested that they are due to shear fracture of the ice at a point where the ice becomes afloat after passing over a rock lip which is higher than the bottom level of the ice when afloat. By applying

a simple beam model, they estimated that the mean shear stress at the rock lip reached a maximum of 7×10^5 N m.$^{-2}$. However, when fracture occurred, the maximum bending stresses would have been seven times larger than the mean shear stress at the rock lip, implying a bending strength for ice of $4{\cdot}5 \times 10^6$ N m.$^{-2}$, which is almost three times greater than values reported by Mantis (1951, p. 24). The actual stresses are expected to be less than those calculated because the ice beam is supported, to an unknown extent, by the surrounding ice shelf.

On the Brunt Ice Shelf, the ice at the hinge line fractures to form individual freely floating icebergs separated by expanses of sea ice. In this case, there is no evidence of a rock step at the hinge line of the type envisaged beneath Beardmore Glacier. The inland ice flows down a steep slope into the sea and at flotation the ice slab experiences an upward bending moment due to the excess of buoyancy forces over weight. Neglecting, for the moment, creep of the ice, an expression will be derived for the bending stress in terms of ice thickness, land-ice slope and seaward length of the slab.

The land ice is regarded as a sheet of ice of thickness H and surface slope α, with its bottom surface extending a distance L into the sea (Fig. 17). Moments are taken about a plane parallel to, and at a

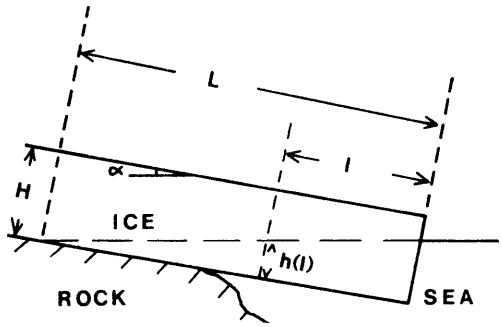

FIGURE 17

Longitudinal section of an ice sheet flowing into the sea.

distance l from, the seaward edge of the slab. The portion of ice thickness below sea-level at this plane is $h(l)$, where

$$h(l) = (L - l) \tan \alpha. \tag{21}$$

For a vertical section of unit width taken parallel to a flow line, the anti-clockwise moment is:

$$M = \int_0^l x \left\{ (h(l) + x \tan \alpha)\, \rho_w g - \rho_i g H \right\} \cos \alpha \, dx \tag{22}$$

and for small α

$$M \sim \{(l^3/3)\, \alpha\, \rho_w + (l^2/2)\, [h(l)\, \rho_w - H\rho_i]\}\, g. \tag{23}$$

M reaches a maximum when

$$\overset{*}{l} = -2\,(H\rho_i - L\alpha\rho_w)/\alpha\, \rho_w \tag{24}$$

and

$$L = \overset{*}{l}/2 + H\rho_i/\alpha\, \rho_w. \tag{25}$$

Thus $\overset{*}{l}$ is twice the distance from the seaward edge to the point where the ice is in hydrostatic equilibrium.

Substituting Equation (25) in Equation (21):

$$h(\overset{*}{l}) = H\rho_i/\rho_w - \overset{*}{l}\alpha/2 \tag{26}$$

and from Equation (23) the maximum bending moment becomes:

$$\hat{M} = \overset{*}{l}^3\, \alpha\rho_w g/12. \tag{27}$$

The maximum bending stress at the bottom of the ice shelf is

$$\hat{\sigma}_b = 6\hat{M}/\overset{*}{H}^2 = \overset{*}{l}^3\, \alpha\rho_w g/2H^2. \tag{28}$$

If it is assumed that fracture occurs at a distance $\overset{*}{l}$ from the seaward edge, then $\overset{*}{l}$ equals the width (l_f) of icebergs forming at the hinge line.

Where the main triangulation scheme crosses the hinge line on the Brunt Ice Shelf, $l_f \sim 350$ m.,

$\alpha \sim 7 \times 10^{-2}$ radians and $H \sim 320$ m., giving the maximum bending stress at the moment of fracture:

$$\hat{\sigma}_b \sim 1{\cdot}5 \times 10^5 \text{ N m.}^{-2}. \tag{29}$$

At the point of flotation there may be a tendency for the land ice to bend downwards due to the decrease of velocity with depth. This would have the effect of increasing the value of α in Equation (28).

By a similar analysis, it can be shown that the maximum *shear* stress averaged over thickness occurs at a distance $l^*/2$ from the seaward edge and its value is approximately $\hat{\sigma}_b/4$ if $l^* \sim H$. The existence of the shear stresses may influence the position at which the fracture takes place so that l_f lies between l^* and $l^*/2$, giving a slightly larger bending stress for a given iceberg size.

At the point where the ice slab becomes afloat, crevasses are likely to form in the bottom surface in the same way that rifts form in an ice shelf down-stream from grounded areas. The penetration "depth" of these crevasses will be limited to the zone of shear near the base of the land ice unless additional tensile stresses are applied, and a bending stress of $1{\cdot}5 \times 10^5$ N m.$^{-2}$ would not be sufficient to extend a crevasse completely through the ice shelf. However, as the crack penetrates the ice, H in Equation (28) decreases causing a rapid increase in $\hat{\sigma}_b$ acting across the crevasse tip, and hence continued propagation of the crack. Equation (28) implies that the maximum bending stress increases rapidly as the ice moves to seaward. However, the effect of creep is to warp upwards the seaward edge of the land ice and, if the floating tongue survives for a sufficiently long period without calving, creep bending will suffice to accommodate completely the change in slope at the hinge line. Thus there is an upper limit to the value of l^* in Equation (28) and its value increases with ice velocity. This, together with the implications of Equation (28), suggests that hinge-line calving is most likely to take place where thin, rapidly moving ice with a steep surface slope flows on to the sea.

IV. MASS BALANCE, PARTICLE PATHS AND BOTTOM MELTING

THE positive side of the mass balance of the Antarctic inland ice sheet can be estimated by measuring surface accumulation rates over a sufficiently large area. The mass balance can then be calculated by subtracting the outflow at the edges of the inland ice sheet. However, it is usually easier to measure outflow near the fronts of the ice shelves, and it then becomes necessary to convert the results into equivalent flow rates across the hinge line. To do this, one needs to know something of the mass flux at both upper and lower surfaces of the ice shelf. So a knowledge of bottom flux contributes not only to an understanding of the ice shelf itself but also to the accuracy of mass-balance estimates for the whole of the Antarctic ice sheet.

Very few reliable estimates of bottom flux have been made. To fit data from the Ross Ice Shelf, Zumberge (1964) suggested that bottom freezing predominated at distances from the ice front greater than 80 km., with a minimum freezing rate of 0·1 m. yr.$^{-1}$ at 130 km. However, assuming all heat absorbed by the ice shelf to be used in warming downward-moving ice and that no heat is supplied by ocean currents, Robin (1968) calculated that the maximum freezing rate would be about 0·02 m. yr.$^{-1}$. So there is ample need for more data, particularly from the central parts of ice shelves. The Brunt Ice Shelf measurements described earlier were used by Thomas and Coslett (1970) to compute a bottom-flux profile extending the whole way from the hinge line to the ice front. Here, equations are derived which can be used to calculate both steady-state and non-steady-state bottom-melting rates. It will also be shown that the inland ice sheet near the Brunt Ice Shelf is approximately in balance, and the trajectories of snow particles falling anywhere between the Brunt Ice Front near Halley Bay and a point 50 km. inland from the hinge line will be calculated.

A. BOTTOM FLUX

Analysis of the temperature/depth curve from the "Little America" bore hole (Wexler, 1960; Crary, 1961; Shumskiy and Zotikov, 1962; Robin, unpublished) led to various estimates of bottom-melting rates beneath the Ross Ice Shelf. An easier approach is by the kinematic method, which involves an independent estimate of the net balance of the ice shelf and hence of the bottom flux necessary to preserve that balance. Steady-state is generally assumed with thickness and mean density a function of position

only. This assumption can, however, be checked by re-measurement at a later date of a known ice thickness or surface-elevation profile. The repeated measurements of Brunt Ice Shelf surface profiles show that, except near the ice front, the steady-state assumption is justified.

Adopting a system of fixed rectangular coordinates with x-axis along a flow line at sea-level and z-axis upwards, the following symbols are defined:

Subscripts s and b refer to upper and lower surfaces respectively.
$q(x)$ = rate of horizontal mass discharge through a section of width $D(x)$.
$\dot{A}(x)$ = accumulation rate expressed as mass per unit area ($(\dot{A}_b)$ is bottom freezing rate).
$u(x)$ = ice-shelf velocity along the relevant flow line (assumed to be independent of z).
$\dot{\epsilon}(x)$ = strain-rate (assuming $\dot{\epsilon}_z = -(\dot{\epsilon}_x + \dot{\epsilon}_y)$).
$\rho(x, z)$ = ice-shelf density.
ρ_w = sea-water density (assumed to be constant).
$\beta(x)$ = bottom slope of the ice shelf (positive for thinning towards the ice front).

For continuity of mass at any point:

$$\frac{\partial q}{\partial x} + \frac{\partial}{\partial t}\int_{Z_b}^{Z_s} D\rho \, dZ = (\dot{A}_s + \dot{A}_b)D \tag{30}$$

or, for steady-state:

$$\frac{\partial q}{\partial x} = (\dot{A}_s + \dot{A}_b)D \tag{31}$$

and

$$q = Du\int_{Z_b}^{Z_s} \rho dZ \tag{32}$$

which, for hydrostatic equilibrium

$$= Du\int_{Z_b}^{o} \rho_w dZ \tag{33}$$

so Equation (31) becomes

$$-Du\rho_w \frac{\partial Z_b}{\partial x} - Z_b\rho_w\left\{D\frac{\partial u}{\partial x} + u\frac{\partial D}{\partial x}\right\} = (\dot{A}_s + \dot{A}_b)D. \tag{34}$$

Since

$$\frac{\partial u}{\partial x} = \dot{\epsilon}_x \text{ and } \frac{\partial D}{\partial x} = \frac{D}{u}\dot{\epsilon}_y, \tag{35}$$

the steady-state condition for mass continuity and hydrostatic equilibrium reduces to

$$\dot{A}_s(x) + \dot{A}_b(x) = \rho_w\{Z_b(x)\,\dot{\epsilon}_z(x) - u(x)\tan\beta(x)\}. \tag{36}$$

So, by measuring $\dot{\epsilon}_x$, $\dot{\epsilon}_y$, $\dot{A}_s$, Z_b and u along a flow line, values of bottom flux along that line can be calculated. Because of the varied composition of the Brunt Ice Shelf, variations in ice thickness across flow lines are pronounced (Fig. 8a) and values of β measured at any angle to the flow line will be in error. The flow line selected was chosen to coincide with the principal drainage from ice stream I and is shown in Fig. 8b, where it can be seen that the middle section of the route along which surface elevations were measured deviated appreciably from this flow line. Associated with this deviation was a rapid drop in surface elevation (Fig. 8a) as the route passed from thick ice shelf originating from ice stream I to ice shelf consisting of cemented icebergs. Isolated estimates of bottom flux deduced from such data would be misleading and the middle section of the surface-elevation profile along the flow line has been interpolated. Within 5 km. of the ice front, elevations were taken from a 1967 plane-table map of the area and are believed accurate to ± 3 m. Fortunately, ice thicknesses were measured by radio echo-sounding (Evans and Smith, 1970) along most of the flow line. These have been reduced to bottom elevations by subtracting the surface elevations. Errors in the resultant bottom profile are largely determined by those of the measured ice thickness (± 10 m.).

By fitting polynomials in x to the measured quantities, a continuous profile of bottom flux was calculated for the entire flow line (Fig. 18). The larger deviations from the regression line in Fig. 18 are

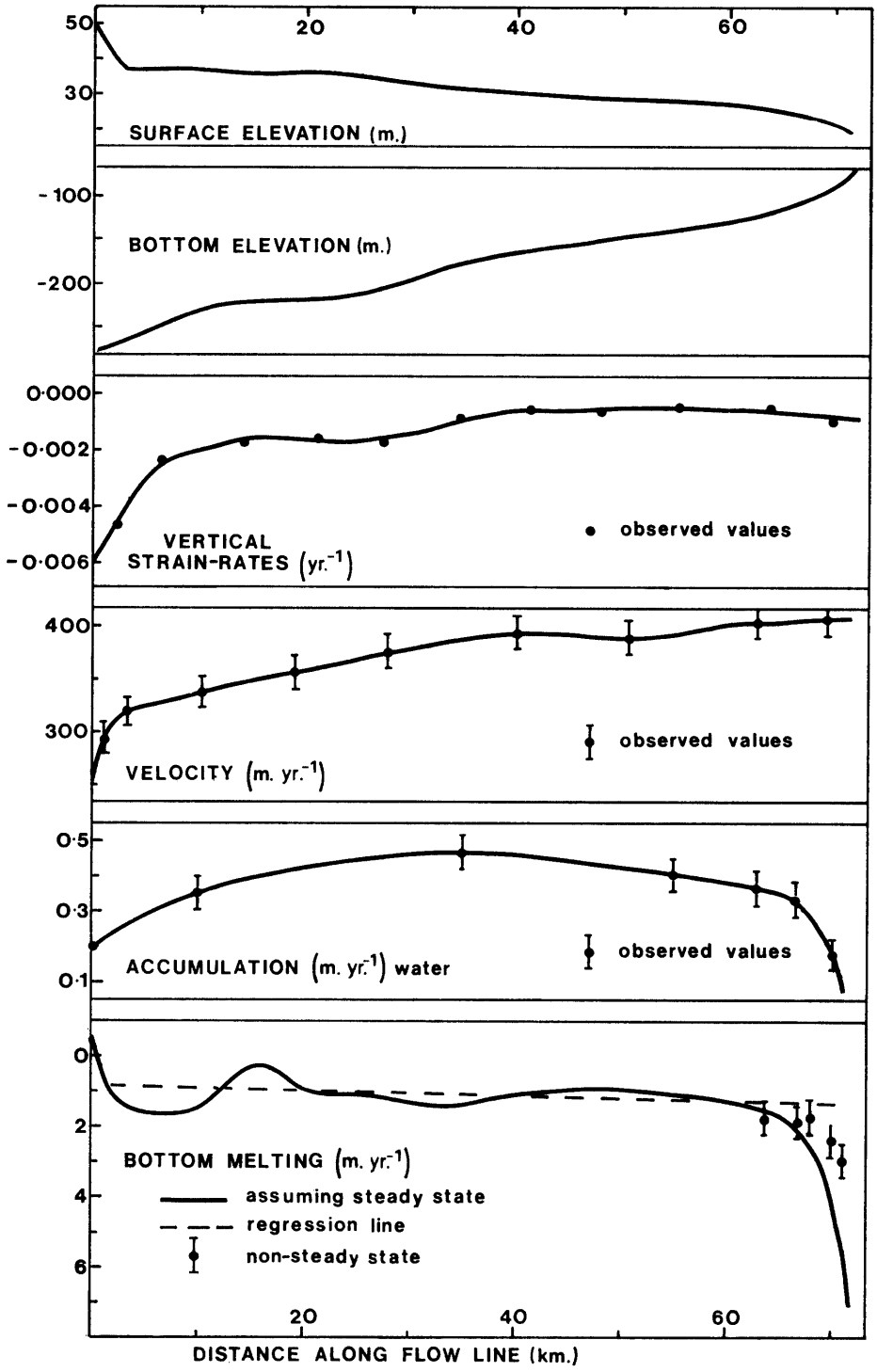

FIGURE 18

Plots of polynomials fitted to the various parameters measured on the Brunt Ice Shelf, and a profile showing melting rates beneath the ice shelf assuming steady-state.

believed to be due to non-steady-state conditions. This is particularly apparent near the ice front where ice-shelf thinning can only be reliably estimated from repeated measurements. Consequently, surface elevations were regularly measured at several points within 10 km. of the Brunt Ice Front and the corresponding bottom-melting rates calculated using the expression derived on p. 34. These values are super-

imposed on the steady-state bottom-melting profile in Fig. 18, and they show a rapid approach to steady-state over the first 10 km. from the ice front.

In Thomas and Coslett (1970), the Brunt Ice Shelf results were compared with the few published estimates of bottom-melting rates for other ice shelves. Most of these were based on measurements over a short distance of surface slope (α) and an assumed value of the variable ratio β/α, the uncertainty of which limited the accuracy of the results. Furthermore, unless measurements were made along a flow line, errors of the type described above may be included. The work on the Brunt Ice Shelf provides the only available profile of bottom-melting rates across an ice shelf, although it is hoped that work recently completed (personal communication from W. F. Budd, February 1970) will give a similar profile for the centre line of the Amery Ice Shelf.

Meanwhile, Thomas and Coslett (1970) have used recent data to compute bottom-melting rates for the Ross and Amery Ice Shelves and, although the scatter in the results is large, there is little evidence for pronounced bottom freezing even at great distances from the ice front. It might be expected that the high melting rates beneath the Brunt Ice Shelf represent an upper limit, since the ice shelf is unbounded and freely exposed to the strong clockwise currents of the Weddell Sea. However, the clearance between sea bed and the bottom of the ice shelf along most of the relevant flow line is probably less than 100 m. Farther south beneath the Filchner Ice Shelf sea depths reach 500–1,000 m. and a larger supply of warm water from the Atlantic deep water is available. This may to some extent explain the very large values of bottom-melting rate deduced by Behrendt (1970) for the Filchner Ice Shelf.

1. *Non-steady-state bottom flux*

In order to compute the profile of bottom-melting rates for the Brunt Ice Shelf, steady-state conditions have been assumed with ice thickness and surface elevation constant at any fixed geographical position. By re-measuring either of these parameters, the validity of the assumption can be tested, and where it fails a more accurate value of bottom flux may be calculated.

Measurements of surface elevation usually refer to the snow surface at some marker fixed in the ice shelf, so a vertical column of ice shelf beneath such a point is considered. Let:

$\dot{A}_m$ = mean annual surface accumulation expressed as mass per unit area.
$\dot{A}$ = annual accumulation observed in the time interval (Δt) between successive measurements of surface elevation.
$\dot{C}$ = annual contraction of the column due to densification of the firn.
$\dot{\epsilon}_z$ = vertical strain-rate ($= -\{\dot{\epsilon}_x + \dot{\epsilon}_y\}$).
ρ_s = mean density of the annual layer nearest the surface.
ρ_i = density of solid ice.
ρ_w = sea-water density (assumed constant).
Z_s = surface elevation. } with respect
Z_b = bottom elevation (negative). } to sea-level
$\dot{M}$ = bottom-melting rate expressed as thickness of solid ice.

The primed values refer to the second set of observations.

Now the column, originally of length L ($= Z_s - Z_b$), can be considered to consist of B m. of air and $(L - B)$ m. of solid ice.

Then for hydrostatic equilibrium:

$$(L - B)\,\rho_i = (L - Z_s)\,\rho_w. \tag{37}$$

Differentiating Equation (37) with respect to time gives:

$$\rho_i\left\{\frac{\partial L}{\partial t} - \frac{\partial B}{\partial t}\right\} = \rho_w\left\{\frac{\partial L}{\partial t} - \frac{\partial Z_s}{\partial t}\right\} \tag{38}$$

or

$$\frac{\partial L}{\partial t} = \left\{\rho_w\frac{\partial Z_s}{\partial t} - \rho_i\frac{\partial B}{\partial t}\right\}\Big/(\rho_w - \rho_i). \tag{39}$$

After an interval Δt, the ice-shelf thickness becomes:

$$L' = L + (\dot{A}/\rho_s)\,\Delta t - \dot{C}\Delta t + L\dot{\epsilon}_z\Delta t - \dot{M}\Delta t \tag{40}$$

and

$$L - L' = (\dot{M} + \dot{C} - \dot{A}/\rho_s - L\dot{\epsilon}_z)\Delta t \sim \{\rho_w(Z_s - Z_s') - \rho_i(B - B')\}/(\rho_w - \rho_i) \tag{41}$$

from Equation (39), so

$$\dot{M} = \frac{\dot{A}}{\rho_s} + L\dot{\epsilon}_z - \dot{C} + \left\{\frac{\rho_w(Z_s - Z_s') - \rho_i(B - B')}{(\rho_w - \rho_i)\Delta t}\right\}. \tag{42}$$

The biggest problem lies in assigning values to $\dot{C}$ and $(B - B')$. The surface accumulation rate varies appreciably with time but the settling rate $\dot{C}$ is unlikely to change in the same way. Thus a period of abnormally high accumulation could result in an increase in surface elevation accompanied by an increase in the air content of the firn. Here $\dot{C}$ is assumed to be controlled by the average accumulation rate over a long period $\dot{A}_m$, such that each year a mean annual accumulation layer is converted into solid ice. $\dot{C}$ then becomes the air content of that layer at the surface. Thus

$$\dot{C} = (\dot{A}_m/\rho_s) - (\dot{A}_m/\rho_i). \tag{43}$$

The decrease in air content of the column after an interval Δt is equal to the contraction due to settling minus the increase due to the air contained in snow accumulated during the interval Δt:

$$B - B' = \left\{\left(\frac{\dot{A}_m}{\rho_s} - \frac{\dot{A}_m}{\rho_i}\right) - \left(\frac{\dot{A}}{\rho_s} - \frac{\dot{A}}{\rho_i}\right)\right\}\Delta t = \left\{\left(\frac{\dot{A}_m - \dot{A}}{\rho_s}\right) - \left(\frac{\dot{A}_m - \dot{A}}{\rho_i}\right)\right\}\Delta t. \tag{44}$$

Combining Equations (42), (43) and (44):

$$\dot{M} = \frac{\rho_w(Z_s - Z_s')}{(\rho_w - \rho_i)\Delta t} + L\dot{\epsilon}_z + \frac{\dot{A}(\rho_w - \rho_s)}{\rho_s(\rho_w - \rho_i)} - \frac{\dot{A}_m(\rho_i - \rho_s)\rho_w}{\rho_i \rho_s (\rho_w - \rho_i)}. \tag{45}$$

This is the expression used to calculate bottom-melting rates at 18 points near the Brunt Ice Front. The values obtained have been grouped according to distance from the ice front and the average of each group is shown in Fig. 18.

If Δt is sufficiently long (say 5 years), $\dot{A}$ tends to $\dot{A}_m$ and:

$$\dot{M} \sim \frac{\rho_w(Z_s - Z_s')}{(\rho_w - \rho_i)\Delta t} + L\dot{\epsilon}_z + \frac{\dot{A}_m}{\rho_i}. \tag{46}$$

2. *Mean value of bottom flux over a large area*

The mean bottom flux $\bar{\dot{F}}$ for a large area of ice shelf can be estimated by considering the mass continuity of a unit vertical section of ice shelf taken along a flow line (Fig. 19). A system of fixed rectangular coordinates is adopted with x-axis along the flow line at sea-level, and z-axis upwards.

Z_s = surface elevation.
Z_b = bottom elevation.
L = length of section.
H = thickness of ice shelf.
$\dot{A}$ = surface-accumulation rate.
$\dot{F}$ = bottom flux.
V = ice-shelf velocity.
ρ = ice-shelf density.

The subscripts 1 and 2 refer respectively to sections P and Q in Fig. 19.

At steady-state, and assuming negligible transverse strain:

$$\int_{Z_{b_1}}^{Z_{s_1}} V_1\rho_1 dz + \int_0^L \dot{A}dx + \int_0^L \dot{F}dx = \int_{Z_{b_2}}^{Z_{s_2}} V_2\rho_2 dz \tag{47}$$

or

$$V_1\bar{\rho}_1 H_1 + \bar{\dot{A}}L + \bar{\dot{F}}L = V_2\bar{\rho}_2 H_2 \tag{48}$$

where the bars imply mean values.

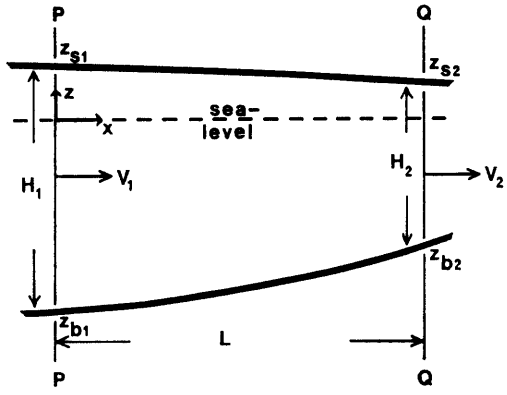

FIGURE 19

Vertical section of an ice shelf taken along a flow line to illustrate symbols used in the calculation of mean bottom flux.

For the Brunt Ice Shelf, taking sections near the hinge line and ice front, respectively:

$V_1 = 323$ m. yr.$^{-1}$ $\quad V_2 = 385$ m. yr.$^{-1}$
$H_1 = 308$ m. $\quad H_2 = 110$ m.
$Z_{s_1} = 43$ m. $\quad Z_{s_2} = 20$ m.

$$\bar{\rho} = \frac{(H - Z_s)}{H} \rho_{sea} \tag{49}$$

so

$\bar{\rho}_1 = 885$ kg. m.$^{-3}$ $\quad \bar{\rho}_2 = 841$ kg. m.$^{-3}$
$\dot{\bar{A}} = 400$ kg. m.^{2} yr.$^{-1}$
$L = 64$ km.

From Equation (48)

$$\bar{\dot{F}} = \frac{V_2\bar{\rho}_2H_2 - V_1\bar{\rho}_1H_1 - \dot{\bar{A}}L}{L} \tag{50}$$

$= -1{,}200$ kg. m.$^{-2}$ yr.$^{-1}$
= bottom melting of 1·35 m. of ice per year.

This is slightly greater than the value given by the bottom-flux profile (Fig. 18), because here it is assumed there is negligible transverse strain. The assumption is more likely to hold for the larger, bounded ice shelves where lateral strain is minimal.

In order to compute a value of mean bottom flux, it is necessary to measure velocity, ice thickness and mean density at only two points along a flow line, together with observations of snow accumulation between these points. Density measurements are likely to be the most difficult to obtain; mean density can be inferred either from the ratio of total thickness to surface elevation or by measuring the variation in density with depth in a bore hole, and it is suggested that any programme of ice-shelf coring should be planned in such a way that an estimate can be made of the mean bottom flux between adjacent bore holes.

3. *Influence of sea currents on bottom-melting rates*

The Amery and Ross Ice Shelves, and indeed most other ice shelves, lie between protective flanks of land ice and the amount of water circulating beneath them is largely dependent on the width of the ice front. Consequently, one should expect bottom-melting rates to be less than beneath the Brunt Ice Shelf. However, virtually nothing is known about sea currents beneath ice shelves and one can only speculate on the distance that they penetrate in from the ice front.

Several attempts have been made to measure sea currents in Halley Bay and the results are summarized in Table III. Whilst the sea temperatures recorded in June 1966 indicate that negligible heat was available for bottom melting during winter, the January temperatures were 0·1° C above freezing point. Using the expression given by Lebedev (1964, p. 121) for heat transfer under conditions of turbulent flow, bottom melting rates at various distances from the ice front can be calculated. Assuming a mean sea

TABLE III

MEASUREMENTS OF SEA CURRENTS AND TEMPERATURES AT VARIOUS DEPTHS IN HALLEY BAY

Source	*Date*	*Method*	*Depth*	*Sea currents*		*Sea temperatures* (°C)
				Velocity (m. sec.$^{-1}$)	*Direction* (° true)	
Deacon, 1964, p. 351	February 1958	Vertically spaced sea electrodes	Mean value for surface to sea bed	0·1	270	–
Unpublished British Antarctic Survey report by C. Dean	August 1961	Horizontally spaced sea electrodes	Mean value near surface	0·35	–	–
Unpublished British Antarctic Survey report by C. Dean	January 1962	Ekman current meter and reversing bottle	Mean values for surface to sea bed	0·25	–	−1·82
Unpublished British Antarctic Survey report by M. Jarman	April 1962	Horizontally spaced sea electrodes	Mean value near surface	0·85	340	–
Unpublished British Antarctic Survey report by W. Izatt	May and June 1966	Horizontally spaced sea electrodes	Mean value near surface	0·2	260	–
Observations made by the author	June 1966	PISA for currents to the sea bed	Sea bed at 210 m.	0·1	300	–
		Resistance thermometer	Mean value from surface to sea bed	–	–	−1·9

current of 200 mm. sec.$^{-1}$, a sea temperature 0·1° C above its freezing point for half the year and a temperature gradient at the bottom of the ice shelf similar to that at "Little America" station (Gow, 1963), the following bottom melting rates are obtained:

1 km. from ice front	3·3 m. of ice per year
10 km. from ice front	2·0 m. of ice per year
100 km. from ice front	1·3 m. of ice per year.

With increasing distance from the ice front, a decrease in both sea temperatures and currents is expected, so the above values should represent upper limits. Nevertheless, the calculation suggests that sufficient heat is available to support the high melting rates deduced for the Brunt Ice Shelf.

Gilmour (1963) and Tressler and Ommundsen (1962) reported measurements of sea currents, temperatures and salinities beneath sea ice at several points in McMurdo Sound throughout the year. From the results, Gilmour estimated an annual southward heat transport through McMurdo Sound of between 1 and 3 $\times$ 10^{18} J. Making the unrealistic assumption that all this heat is used in melting a uniform layer from the underside of the entire Ross Ice Shelf, an annual loss of between 6 and 19 mm. of ice is found from this heat source alone.

B. MASS BALANCE OF THE INLAND ICE SHEET NEAR THE BRUNT ICE SHELF

The mass balance of any bounded area of the Antarctic ice sheet is the net surface accumulation minus the net loss of ice across the boundaries. If catchment areas separated by the crests of intervening ridges are considered, flow of ice across the boundaries can only take place to seaward. Then the accuracy of any estimate of mass balance for an individual catchment area is limited by lack of knowledge of its geographical boundaries, of surface accumulation rates and of the total outflow. To improve the accuracy this study can be further limited to consider a unit vertical section through the catchment area

perpendicular to the surface contours. If the flow lines are parallel, then the mass balance of this section is the net surface accumulation minus the outflow to seaward. For the Brunt Ice Shelf catchment area the position of the summit of the ridge to the south of the ice-movement scheme is reliably known from several oversnow traverses, and a metre wide section (AA′ in Fig. 20) through the stake network is considered. Ice thicknesses along the entire section are also known from the work of Bailey (Bailey and Evans, 1968) and the more recent radio echo sounding described on p. 11. From Nye (1952, p. 84), it can be shown that, if zero bottom sliding is assumed, the velocity of the ice column averaged over its depth is $(n + 1)/(n + 2)$ times the surface velocity, where n is the flow-law exponent. The surface velocity at A in Fig. 20 is 50 m. yr.$^{-1}$, so if $n = 3$ the mean velocity is 40 m. yr.$^{-1}$. The height of the ice column is 1,000 m., giving a total annual outflow through A of 4×10^4 m.^{3} of ice.

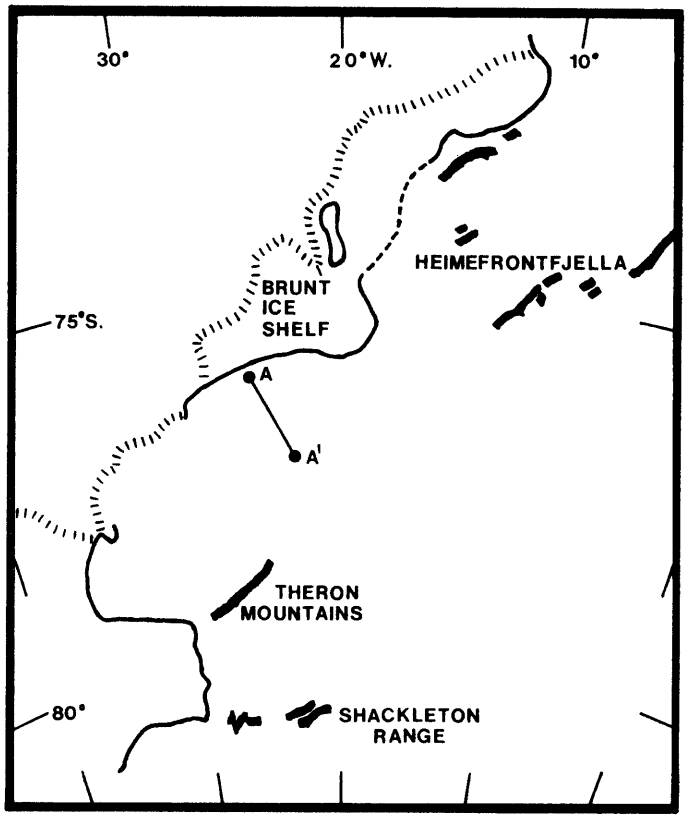

FIGURE 20

The Brunt Ice Shelf and adjacent inland ice sheet.

Mean snow accumulation of the drainage area was obtained from measurements every 3–4 km. along the route from Halley Bay to the Theron Mountains (Fig. 20) in 1967 and along the route from Halley Bay to the Shackleton Range in 1969. From Fig. 3 it can be seen that at Halley Bay 1967 was a dry year, whilst 1969 was a relatively wet one. Therefore, values have been adjusted to more representative long-period estimates assuming that variations with time in accumulation recorded at Halley Bay are also typical of the inland ice sheet.

In Table IV the contributions to the mass balance of the section AA′ are listed. The difference between total accumulation and total outflow is about 6 per cent, considerably less than the estimated error; so it is concluded that within the limits of error this area of the inland ice sheet is in balance. Although this result represents the mass balance of only a small area of the Antarctic ice sheet, it is based on measurements of all the relevant parameters, in particular of the drainage rate across the hinge line.

Giovinetto (1970) suggested that the Antarctic ice sheet is responding bi-modally to the present climatic regime, the interior region having a positive mass balance whilst the peripheral region has a larger negative one to balance the observed rise in sea-level. Independent evidence reviewed by Hollin (1970)

TABLE IV
MASS BALANCE OF THE INLAND ICE SHEET NEAR HALLEY BAY

			Probable error (per cent)
Adjusted mean accumulation rate	Theron Mountains route	0·30 m. ice yr.$^{-1}$	±10
	Shackleton Range route	0·38 m. ice yr.$^{-1}$	±10
Resultant mean		0·34 m. ice yr.$^{-1}$	±20
Drainage area up-stream of A in Fig. 20		$1{\cdot}1\times10^{5}$ m.^{2}	Negligible
Total accumulation rate for unit width of inland ice sheet taken along a flow line		$3{\cdot}8\times10^{4}$ m.^{3} ice yr.$^{-1}$	±20
Total outflow past A (see p. 38)		4×10^{4} m.^{3} ice yr.$^{-1}$	±20

supports the view that the interior of the ice sheet is thickening, but over a larger area than that proposed by Giovinetto. Furthermore, the results of the present work suggest that the Brunt Ice Shelf drainage area, which is within Giovinetto's peripheral zone, is approximately in balance. It would appear then that the negative-balance zone may be considerably smaller than that envisaged by Giovinetto, implying a very rapid thinning rate within the zone. However, Giovinetto's analysis assumed (following Zumberge, 1964) net freezing beneath the major ice shelves, whereas the present results suggest that appreciable bottom melting may be more widespread than previously suspected. Even a small net melting rate would reduce the positive budget of Giovinetto's interior zone and hence also the negative budget assigned to the peripheral zone.

Before anything more precise can be concluded more data are needed. Estimates of accumulation rates over the inland ice sheet must be improved, a velocity profile should be measured across the Filchner Ice Shelf, and efforts should be made to measure bottom flux in the interior of the larger ice shelves. On p. 36 a method is proposed by which mean bottom flux could be estimated for large areas of an ice shelf with a minimum of observations.

C. PARTICLE PATHS

To calculate particle paths through the ice shelf, rectangular axes with x-axis along a flow line at the surface, and z-axis downward are taken (Fig. 21).

V = ice-shelf velocity ($= V(x)$ m. yr.$^{-1}$).
$\dot{\epsilon}_z$ = vertical strain-rate ($= \dot{\epsilon}_z(x) = -\{\dot{\epsilon}_x + \dot{\epsilon}_y\}$ yr.$^{-1}$).
$\dot{A}$ = accumulation rate ($= \dot{A}(x)$ kg. m.$^{-2}$ yr.$^{-1}$).
ρ = density ($= \rho(z)$, and $\rho(0)$ = density of surface snow).
D_1 = thickness of an annual layer at the surface ($= D_1(x)$).
D_n = thickness of an annual layer after n years ($= D_n(x)$).

The following assumptions are made:

i. The velocity measured at the surface is representative of that at depth. This is true for the ice shelf and it is a fair approximation for near-surface land ice.
ii. The function $\rho(z)$ is independent of time (Sorge's Law)—see p. 7—and of x.
iii. The functions $\dot{A}(x)$, $V(x)$ and $\dot{\epsilon}_z(x)$ are independent of time.

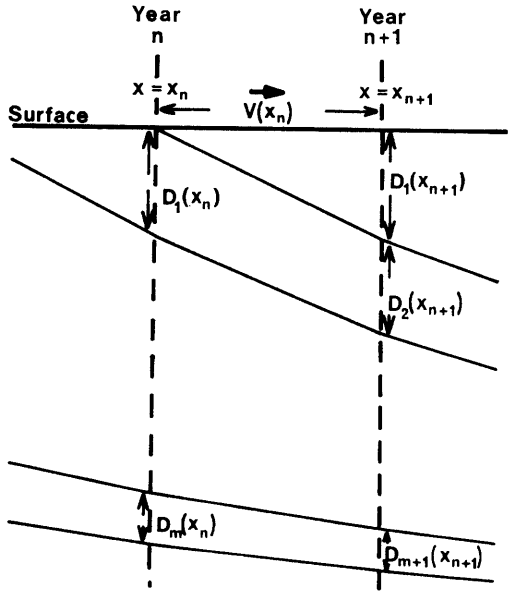

FIGURE 21

Vertical section taken along a flow line to illustrate symbols used in particle-path calculations.

If the origin is taken at the point of deposition of the relevant snow particle, then after m years

$$x = x_m = \sum_{i=0}^{i=m-1} V(x_i) \tag{51}$$

and its depth below the surface is

$$z = \sum_{i=1}^{=m} D_i(x_m), \tag{52}$$

where

$$D_1(x_m) \sim \dot{A}(x_m)/\rho(0)$$
$$D_2(x_m) \sim \frac{\dot{A}(x_{m-1})}{\rho(D_1(x_m))}\left\{1 + \dot{\epsilon}_z(x_{m-1})\right\} = \frac{D_1(x_{m-1})\,\rho(0)\,(1 + \dot{\epsilon}_z(x_{m-1}))}{\rho(D_1(x_m))} \tag{53}$$

and

$$D_{i+1}(x_m) \sim \frac{D_i(x_{m-1})\,\rho\left\{\sum_{n=1}^{n=i-1} D_n(x_{m-1})\right\}(1 + \dot{\epsilon}_z(x_{m-1}))}{\rho\left\{\sum_{n=1}^{n=i} D_n(x_m)\right\}}. \tag{54}$$

Using a computer, Equations (51) and (52) were solved iteratively to give the paths taken by any snow particle falling between a point 50 km. south of the hinge line and the Brunt Ice Front. Account was taken of variations in $\dot{A}$, V and $\dot{\epsilon}_z$ by expressing each as a polynomial in x. Variation of density with depth has sometimes been neglected in particle trajectory calculations (Crary and others, 1962, p. 130; Budd, 1969, p. 182), its effect being small compared with ice thickness. On an ice shelf, however, the initial rapid descent of snow particles due to densification of the firn is significant. For the Brunt Ice Shelf, the density/depth relationship found at Maudheim (equation 1 from Schytt (1958*b*, p. 120)) has been adapted to yield a mean density equal to that observed on the Brunt Ice Shelf, giving:

$$\rho(z) = 917 - 467e^{-0{\cdot}05z} \text{ kg. m.}^{-3} \text{ with } z \text{ in m.} \tag{55}$$

In Fig. 22 the results are plotted as particle paths with a time interval between each of 200 yr. The ages marked are those of particles at the ice front. Snow falling at the hinge line takes approximately 190 yr. to reach the ice front, where it is at a depth of 93 m. below the surface and 75 m. below sea-level. Where the trajectories cut the bottom of the ice shelf, the particle has been lost by bottom melting. 10 km. from the ice front the bottom of the ice shelf is about 1,000 yr. old and originated at a point 50 km. inland from

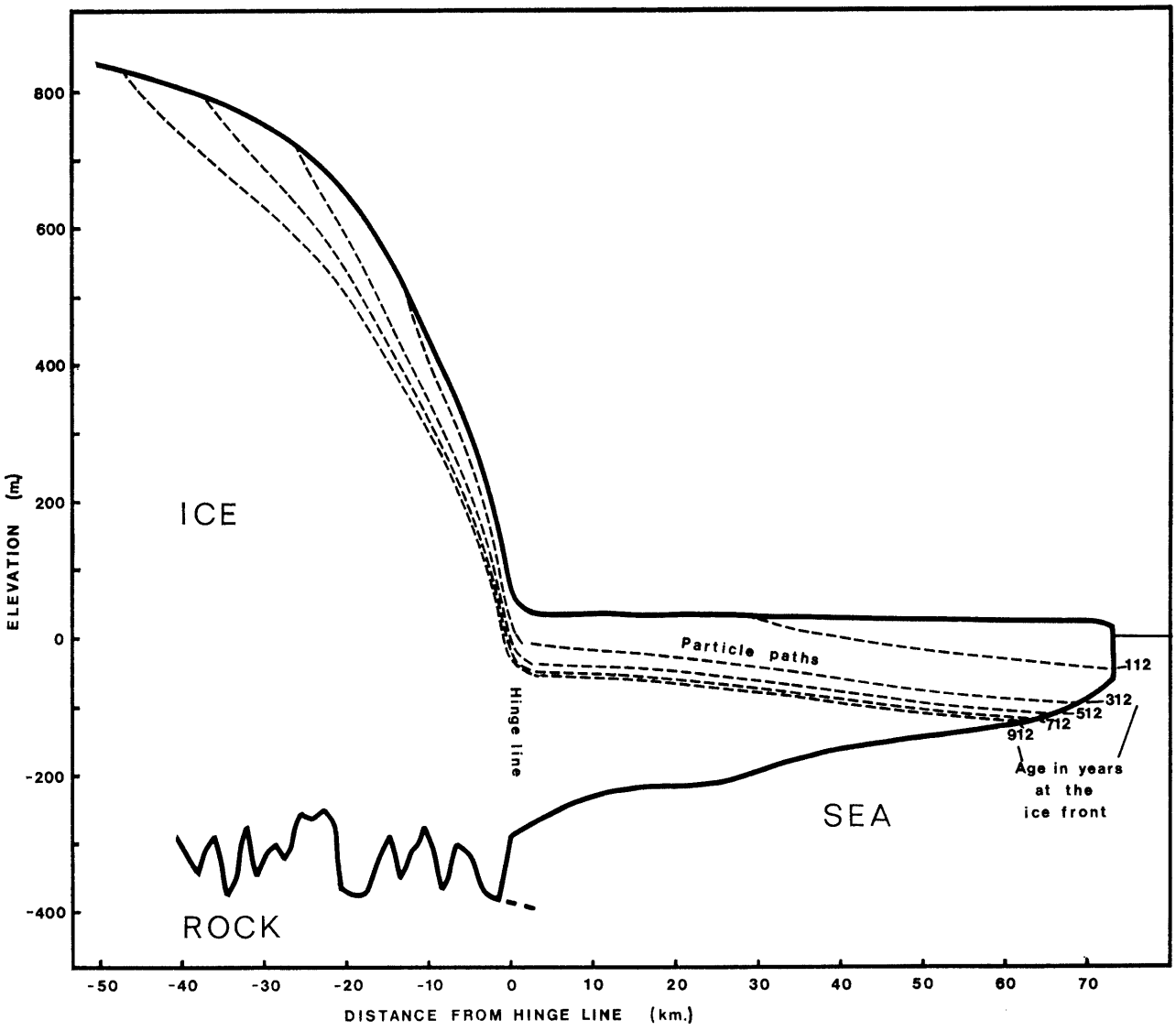

FIGURE 22

Particle paths along the flow line which passes through Halley Bay station. The vertical exaggeration is about 80 : 1.

the hinge line. However, bottom melting near the ice front is so rapid that the bottom of the ice shelf at the ice front is only 220 yr. old and originated at a point 5 km. inland from the hinge line. None of the snow falling at distances greater than 5 km. inland from the hinge line ever reaches the ice front.

V. CONCLUSIONS AND SUGGESTIONS FOR FURTHER WORK

OBSERVATIONS made on the Brunt Ice Shelf enable one to estimate not only the mass balance at the upper surface but also the rate of melting from beneath the ice shelf. The same observations have been used (Thomas, 1973*a*, *b*) to examine the creep behaviour of ice at low stresses. Thus ice shelves provide excellent tools with which to investigate the behaviour both of the Antarctic ice sheet and of ice as a material. The high melting rates calculated at all points beneath the Brunt Ice Shelf suggest that bottom melting may be more widespread than previously suspected and an accurate assessment of the mass

balance of Antarctica must await the calculation of bottom-melting profiles across the major ice shelves. The Brunt Ice Shelf observations were made from a closely spaced network of stations and gave detailed information along a relatively short flow line. On the larger ice shelves, with flow lines of several hundred kilometres in length, the necessary observations could be reduced to:

i. Strain-rates measured at a series of known positions along a flow line. Within 150 km. of the ice front these measurements should be made at 20 km. intervals, thereafter at 50–100 km. intervals.
ii. Absolute ice velocity determined at one, at least, of the stations.
iii. Measurements of surface elevation and ice-thickness profiles along the flow line.

Ideally, holes should be drilled through the ice shelf at two or three selected stations to supply data on the variation of temperature and density with depth. If this is done, the measurements of surface elevation can be omitted. The proposed Ross Ice Shelf drilling project (Zumberge, 1971) presents an excellent opportunity to relate bore-hole information to surface measurements of the kind described above.

In a review of possible calving mechanisms it has been concluded that:

i. Stresses induced by tidal rise and fall are sufficient to explain the occurrence of strand cracks at or near to the hinge line, but complete fracture is unlikely except in areas of large tidal range.
ii. Stresses induced by the unbalanced moment at the ice front may result in calving of prismatic icebergs with width approximately equal to ice thickness. The time interval between calving depends largely on the fracture criteria for ice. This type of calving should be preceded by an arching of the ice-shelf surface near the ice front, and a repeated series of level traverses perpendicular to a fresh ice front could detect whether this is taking place. Observations on existing ice fronts indicate that calving of small icebergs is seldom able to keep pace with ice movement.
iii. Under the influence of a tsunami with appropriate period, large stresses could be induced within a floating ice sheet vibrating at its natural frequency or at one of the harmonics. As a first test of this possibility one should search for a correlation between the timing of major calving events as revealed by satellite photography and the occurrence of tsunamis. More direct evidence would be supplied by recording gravimeters installed on suitably exposed tongues of ice shelf.
iv. In most cases, stresses induced within an ice shelf by the action of sea currents are small. However, the prolonged action of such stress may be a contributory factor in the calving of long tongues of floating ice that are joined to the main body of ice shelf by a narrow intact "neck".

Finally, it should be noted that many of the problems associated with iceberg calving cannot be solved until more is known about the fracture criteria for ice in terms of stress, temperature and period of loading.

VI. ACKNOWLEDGEMENTS

THE processing and interpretation of the data used in this report were carried out during 1968–72 at the Scott Polar Research Institute under the supervision of Dr. C. W. M. Swithinbank, to whom I am greatly indebted. I should also like to express my gratitude to Dr. G. de Q. Robin, the staff of, and visitors to, the Scott Polar Research Institute for providing working conditions which, in any of the bigger more specialized institutions, it would be impossible to better.

Dr. B. M. Ewen Smith patiently extricated me from many computer programme problems, and I have greatly benefited from helpful discussions with Dr. J. G. Paren and Dr. J. C. F. Walker. I am particularly indebted to A. Johnston, who gave me much useful advice on survey techniques.

Most of the field data from the Brunt Ice Shelf were obtained with the help of many field assistants: B. Armstrong, A. Baker, C. Blossom, M. Burgin, P. Coslett, R. Docchar, C. Gostick, W. Izatt, R. Lloyd, C. M. Read, M. J. Skidmore, A. Smith, P. Wharton, A. Wilson and C. Wornham. P. Coslett kindly supplied the 1967 and 1968 results of levelling across the ice shelf. Other data were gathered by N. Riley, R. Wells, A. C. Wager, D. Peel, J. Jamieson, M. Guyatt and A. Clayton. To all these, and to many other Survey personnel, I give my sincere thanks.

VII. REFERENCES

ANONYMOUS. 1969. Kaart van omgewing te SANAE. *Antarkt. Bull.*, No. 29, 61–63.

ARDUS, D. A. 1965*a*. Morphology and regime of the Brunt Ice Shelf and the adjacent inland ice, 1960–61. *British Antarctic Survey Bulletin*, No. 5, 13–42.

————. 1965*b*. Surface deformation, absolute movement and mass balance of the Brunt Ice Shelf near Halley Bay, 1961. *British Antarctic Survey Bulletin*, No. 6, 21–41.

BAILEY, J. T. *and* S. EVANS. 1968. Radio echo-sounding on the Brunt Ice Shelf and in Coats Land, 1965. *British Antarctic Survey Bulletin*, No. 17, 1–12.

BARCLAY, L. W. 1964. Sledging and surveying. (*In* BRUNT, D., *ed. The Royal Society International Geophysical Year Antarctic Expedition, Halley Bay, Coats Land, Falkland Islands Dependencies, 1955–59. IV. Meteorology, glaciology, appendixes.* London, Royal Society, 329–38.)

BARDIN, V. I. *and* V. I. SHIL'NIKOV. 1960. "Produktivnost" berega vostochnoy Antarktidy ["Productivity" of the coast of east Antarctica]. *Inf. Byull. sov. antarkt. Eksped.*, No. 23, 28–32. [English translation: Vol. 3 (1965), 100–03.]

BEHRENDT, J. C. 1962. Geophysical and glaciological studies in the Filchner Ice Shelf area of Antarctica. *J. geophys. Res.*, **67**, No. 1, 221–34.

————. 1970. The structure of the Filchner Ice Shelf and its relation to bottom melting. (*In* GOW, A. J., KEELER, C., LANGWAY, C. C. *and* W. F. WEEKS, *ed. International Symposium on Antarctic Glaciological Exploration (ISAGE) ... 1968 ....* Gentbrugge, International Association of Scientific Hydrology, etc., 488–96.) [IASH Publication No. 86.]

BENDER, J. A. *and* A. J. GOW. 1961. Deep drilling in Antarctica. *Gen. Assembly int. Un. Geod. Geophys., Helsinki, 1960. Int. Assoc. sci. Hydrol.*, 132–41. [IASH Publication No. 55.]

BIOT, M. A. 1959. The influence of gravity on the folding of a layered viscoelastic medium under compression. *J. Franklin Inst.*, **267**, No. 3, 211–28.

BLACKWELL, M. J. 1960. Recent scientific activities at Halley Bay: International Geophysical Co-operation, 1959. *Nature, Lond.*, **187**, No. 4742, 982–84.

BUDD, W. F. 1966. The dynamics of the Amery Ice Shelf. *J. Glaciol.*, **6**, No. 45, 335–58.

————. 1969. The dynamics of ice masses. *A.N.A.R.E. Sci. Rep.*, Ser. A (IV), Glaciology, No. 108, 216 pp.

CAMPBELL, W. J. 1965. The wind-driven circulation of ice and water in a polar ocean. *J. geophys. Res.*, **70**, No. 14, 3279–301.

COLLINS, I. F. *and* C. SWITHINBANK. 1968. Rifts at the foot of the Beardmore Glacier, Antarctica. *Gen. Assembly int. Un. Geod. Geophys., Berne, 1967. Int. Assoc. sci. Hydrol.*, 109–14. [IASH Publication No. 79.]

CRARY, A. P. 1961. Glaciological studies at Little America station, Antarctica, 1957 and 1958. *IGY glaciol. Rep. Ser.*, No. 5, 197 pp.

————., ROBINSON, E. S., BENNETT, H. F. *and* W. W. BOYD. 1962. Glaciological studies of the Ross Ice Shelf, Antarctica, 1957–1960. *IGY glaciol. Rep. Ser.*, No. 6, 193 pp.

DEACON, G. E. R. 1964. Sea current measurements. (*In* BRUNT, D., *ed. The Royal Society International Geophysical Year Antarctic Expedition, Halley Bay, Coats Land, Falkland Islands Dependencies, 1955–59. IV. Meteorology, glaciology, appendixes.* London, Royal Society, 348–52.)

DEFANT, A. 1961. *Physical oceanography. Vol. 2.* Oxford, Pergamon Press.

DORRER, E., HOFMANN, W. *and* W. SEUFERT. 1969. Geodetic results of the Ross Ice Shelf survey expeditions, 1962–63 and 1965–66. *J. Glaciol.*, **8**, No. 52, 67–90.

DORSEY, N. E. 1940. *Properties of ordinary water-substance in all its phases: water vapor, water and all the ices.* New York, Reinhold. [American Chemical Society. Monograph Series, No. 81.]

EVANS, S. *and* B. M. E. SMITH. 1970. Radio echo exploration of the Antarctic ice sheet. 1969–70. *Polar Rec.*, **15**, No. 96, 336–38.

FLEET, M. 1965. The occurrence of rifts in the Larsen Ice Shelf near Cape Disappointment. *British Antarctic Survey Bulletin*, No. 6, 63–66.

GILMOUR, A. E. 1963. Hydrological heat and mass transport across the boundary of the ice shelf in McMurdo Sound, Antarctica. *N.Z. Jl Geol. Geophys.*, **6**, No. 3, 402–22.

GIOVINETTO, M. B. 1970. The Antarctic ice sheet and its probable bimodal response to climate. (*In* GOW, A. J., KEELER, C., LANGWAY, C. C. *and* W. F. WEEKS, *ed. International Symposium on Antarctic Glaciological Exploration (ISAGE) ... 1968 ....* Gentbrugge, International Association of Scientific Hydrology, etc., 347–58.) [IASH Publication No. 86.]

GOW, A. J. 1963. The inner structure of the Ross Ice Shelf at Little America V, Antarctica, as revealed by deep core drilling. *Gen. Assembly int. Un. Geod. Geophys., Berkeley, 1963. Int. Assoc. sci. Hydrol.*, 272–84. [IASH Publication No. 61.]

HARRISON, C. H. 1970. Reconstruction of sub-glacial relief from radio echo sounding records. *Geophysics*, **55**, No. 6, 1099–115.

HOCHSTEIN, M. P. *and* G. F. RISK. 1967. Geophysical measurements on the McMurdo Ice Shelf, Antarctica, during 1965–66. *Rep. Geophys. Div. N.Z. Dep. scient. ind. Res.*, No. 47, 82 pp.

HOLDSWORTH, G. 1969*a*. Primary transverse crevasses. *J. Glaciol.*, **8**, No. 52, 107–29.

————. 1969*b*. Flexure of a floating ice tongue. *J. Glaciol.*, **8**, No. 54, 385–97.

————. 1970. Deformation of the Ross Ice Shelf: comments. *Geol. Soc. Am. Bull.*, **81**, No. 5, 1569–70.

HOLLIN, J. T. 1970. Is the Antarctic ice sheet growing thicker? (*In* GOW, A. J., KEELER, C., LANGWAY, C. C. *and* W. F. WEEKS, *ed. International Symposium on Antarctic Glaciological Exploration (ISAGE) ... 1968 ....* Gentbrugge, International Association of Scientific Hydrology, etc., 363–74.) [IASH Publication No. 86.]

JENSSEN, D. *and* U. RADOK. 1961. Transient temperature distributions in ice caps and ice shelves. *Gen. Assembly int. Un. Geod. Geophys., Helsinki, 1960. Int. Assoc. sci. Hydrol.*, 112–22. [IASH Publication No. 55.]

KEHLE, R. 1964. Deformation of the Ross Ice Shelf, Antarctica. *Geol. Soc. Am. Bull.*, **75**, No. 5, 259–86.

KONOVALOV, G. V. 1963. Deflyatsionyye vpadiny na shel'fovom lednike Lazareva [Deflation hollows on the Lazarev ice shelf]. *Inf. Byull. sov. antarkt. Eksped.*, No. 39, 9–12. [English translation: Vol. 4, No. 39 (1964), 263–65.]

KRUCHININ, YU. A. 1965. *Shel'fovye ledniki Zemli Korolevy Mod [Ice shelves of Dronning Maud Land]*. Leningrad, Gidrometeorologicheskoe Izdatel'stvo. [English translation: Jerusalem, Israel Program for Scientific Translations, 1969.]

LEBEDEV, V. L. 1964. Teploobmen mezhdu antarkticheskimi vodami aysbergami i lednikami [Heat exchange between Antarctic waters, icebergs, and glaciers]. (*In Antarktika. Doklady komissii, 1963.* Moskva, Izdatel'stvo Akademie Nauk SSSR, 106–21.) [English translation: *Antarctica. Commission reports, 1963.* Jerusalem, Israel Program for Scientific Translations, 1966, 111–27.]

LEDENEV, V. G. *and* A. P. YEVDOKIMOV. 1965. Izmeneniya shel'fovykh lednikov Zapadnogo i Eymeri [Changes in the West and Amery Ice Shelves]. *Inf. Byull. sov. antarkt. Eksped.*, No. 55, 12–18. [English translation: Vol. 6, No. 55 (1966), 4–7.]

LIMBERT, D. W. S. 1963. The snow accumulation budget at Halley Bay in 1959, and associated meteorological factors. *British Antarctic Survey Bulletin*, No. 2, 73–92.

———. 1964. The absolute and relative movement, and regime of the Brunt Ice Shelf near Halley Bay. *British Antarctic Survey Bulletin*, No. 3, 1–11.

LOEWE, F. 1969. Calving from floating glaciers: comment on Dr N. Reeh's paper. *J. Glaciol.*, **8**, No. 53, 321–22.

LUNDE, T. 1961. On the snow accumulation in Dronning Maud Land. *Skr. norsk Polarinst.*, No. 123, 48 pp.

MACDOWALL, J. 1964. Glaciological observations. Part I. Glaciological observations at the base. (*In* BRUNT, D., *ed. The Royal Society International Geophysical Year Antarctic Expedition, Halley Bay, Coats Land, Falkland Islands Dependencies, 1955–59. IV, Meteorology, glaciology, appendixes.* London, Royal Society, 269–313.)

———., BARCLAY, L. W. *and* J. M. C. BURTON. 1964. Glaciological observations. Part II. Glaciological observations during sledging journeys. (*In* BRUNT, D., *ed. The Royal Society International Geophysical Year Antarctic Expedition, Halley Bay, Coats Land, Falkland Islands Dependencies, 1955–59. IV. Meteorology, glaciology, appendixes.* London, Royal Society, 314–28.)

MANTIS, H. T., *ed.* 1951. Review of the properties of snow and ice. *S.I.P.R.E. Rep.*, No. 4, 156 pp.

MEIER, M. F. 1958. The mechanics of crevasse formation. *Gen. Assembly int. Un. Geod. Geophys., Toronto, 1957. Int. Assoc. sci. Hydrol.*, 500–08. [IASH Publication No. 46.]

NYE, J. F. 1952. The mechanics of glacier flow. *J. Glaciol.*, **2**, No. 12, 82–93.

PATERSON, W. S. B. 1969. *The physics of glaciers.* Oxford, Pergamon Press.

REEH, N. 1968. On the calving of ice from floating glaciers and ice shelves. *J. Glaciol.*, **7**, No. 50, 215–32.

———. 1970. Natural frequency of the system of a heavy elastic plate covering shallow water. *Bygningsst. Meddr*, **41**, No. 3, 167–87.

ROBIN, G. DE Q. 1955. Ice movement and temperature distribution in glaciers and ice sheets. *J. Glaciol.*, **2**, No. 18, 523–32.

———. 1958. Glaciology. III. Seismic shooting and related investigations. *Norw.-Br.-Swed. Antarct. Exped., Scient. Results*, **5**, 3–134.

———. 1960. Some comments on the temperature distribution in ice shelves. *Union Géodésique et Géophysique Internationale, Monographie* No. 5, 67. [Antarctic Symposium, Buenos Aires, 17–25 Novembre 1959.]

———. 1968. [Contribution to discussion.] *Gen. Assembly int. Un. Geod. Geophys., Berne, 1967. Int. Assoc. sci. Hydrol.*, 265. [IASH Publication No. 79.]

SCHYTT, V. 1958*a*. Glaciology. II. Snow studies at Maudheim. *Norw.-Br.-Swed. Antarct. Exped., Scient. Results*, **4A**, 1–63.

———. 1958*b*. Glaciology. II. The inner structure of the ice shelf at Maudheim as shown by core drilling. *Norw.-Br.-Swed. Antarct. Exped., Scient. Results*, **4C**, 113–51.

———. 1960. Glaciology. II. Snow and ice temperatures in Dronning Maud Land. *Norw.-Br.-Swed. Antarct. Exped., Scient. Results*, **4D**, 153–79.

SHUMSKIY, P. A. *and* I. A. ZOTIKOV. 1963. O donnom tayanii shel'fovykh lednikov Antarktidy [Bottom melting of ice shelves in Antarctica]. (*In Antarktika. Doklady komissii, 1962.* Moskva, Izdatel'stvo Akademie Nauk SSSR, 87–108.) [English translation: *Antarctica. Commission reports, 1962.* Jerusalem, Israel Program for Scientific Translations, 1969, 90–112.]

SORGE, E. 1935. Glaziologische Untersuchungen in Eismitte. *Wiss. Ergebn. dt. Grönland-Exped. Alfred Wegener*, **3**, 62–270.

STUART, A. W. *and* C. BULL. 1963. Glaciological observations on the Ross Ice Shelf near Scott Base, Antarctica. *J. Glaciol.*, **4**, No. 34, 399–414.

SUYETOVA, I. A. 1962. Kartometriya Antarktidy [Cartometry in Antarctica]. (*In Antarktika. Doklady komissii, 1961.* Moskva, Izdatel'stvo Akademie Nauk SSSR, 7–11.) [English translation: *Antarctica. Commission reports, 1961.* Jerusalem, Israel Program for Scientific Translations, 1966, 1–5.]

SWITHINBANK, C. W. M. 1957*a*. Glaciology. I. The morphology of the ice shelves of western Dronning Maud Land. *Norw.-Br.-Swed. Antarct. Exped., Scient. Results*, **3A**, 1–37.

SWITHINBANK, C. W. M. 1957*b*. Glaciology. I. The regime of the ice shelf at Maudheim as shown by stake measurements. *Norw.-Br.-Swed. Antarct. Exped., Scient. Results*, **3B**, 41–75.

————. 1958. Glaciology. I. The movement of the ice shelf at Maudheim. *Norw.-Br.-Swed. Antarct. Exped., Scient. Results*, **3C**, 77–96.

————. 1960. Maudheim revisited: the morphology and regime of the ice shelf, 1950–1960. *Årbok norsk Polarinst.*, 1960, 28–31.

————. 1963. Ice movement of valley glaciers flowing into the Ross Ice Shelf, Antarctica. *Science, N.Y.*, **141**, No. 3580, 523–24.

————. *and* J. H. ZUMBERGE. 1965. The ice shelves. (*In* HATHERTON, T., *ed. Antarctica.* London, Methuen & Co., 199–220.)

THIEL, E., CRARY, A. P., HAUBRICH, R. A. *and* J. C. S. BEHRENDT. 1960. Gravimetric determination of ocean tide, Weddell and Ross Seas, Antarctica. *J. geophys. Res.*, **65**, No. 2, 629–36.

THOMAS, R. H. 1970. Survey on moving ice. *Surv. Rev.*, **20**, No. 157, 322–38.

————. 1971. Flow law for Antarctic ice shelves. *Nature, Lond. (Phys. Sci.)*, **232**, No. 30, 85–87.

————. 1973*a*. The creep of ice shelves: theory. *J. Glaciol.*, **12**, No. 64, 45–53.

————. 1973*b*. The creep of ice shelves: interpretation of observed behaviour. *J. Glaciol.*, **12**, No. 64, 55–70.

————. *and* P. H. COSLETT. 1970. Bottom melting of ice shelves and the mass balance of Antarctica. *Nature, Lond.*, **228**, No. 5266, 47–49.

TRESSLER, W. L. *and* A. M. OMMUNDSEN. 1962. Seasonal oceanographic studies in McMurdo Sound, Antarctica. *Tech. Rep. hydrogr. off., Wash.*, No. 125, 141 pp.

WEERTMAN, J. 1957. Deformation of floating ice shelves. *J. Glaciol.*, **3**, No. 21, 38–42.

————. 1973. Can a water-filled crevasse reach the bottom surface of a glacier? (*In Symposium on the hydrology of glaciers, Cambridge, 7-13 September 1969. Organized by the Glaciological Society*, 139-45). [IASH Publication No. 95.]

WEXLER, H. 1960. Heating and melting of floating ice shelves. *J. Glaciol.*, **3**, No. 27, 626–45.

WIEGEL, R. L. 1964. *Oceanographical engineering.* Englewood Cliffs, Prentice-Hall. [Series in fluid mechanics.]

WILSON, G. 1960. The tectonics of the "great ice chasm", Filchner Ice Shelf, Antarctica. *Proc. Geol. Ass.*, **71**, No. 2, 130–38.

WRIGHT, C. S. *and* R. E. PRIESTLEY. 1922. *Glaciology.* London, Harrison and Sons, Ltd. [British (Terra Nova) Antarctic Expedition, 1910–1913.]

ZOTIKOV, I. A. 1964. O temperaturakh v tolshche lednikov Antarktidy [Temperatures inside Antarctic glaciers]. (*In Antarktika. Doklady komissii, 1963.* Moskva, Izdatel'stvo Akademie Nauk SSSR, 61–105.) [English translation: *Antarctica. Commission reports, 1963.* Jerusalem, Israel Program for Scientific Translations, 1966, 64–110.]

ZUMBERGE, J. H. 1964. Horizontal strain and absolute movement of the Ross Ice Shelf between Ross Island and Roosevelt Island, Antarctica, 1958–1963. (*In* MELLOR, M., *ed. Antarctic snow and ice studies.* Washington, D.C., American Geophysical Union, 65–81.) [Antarctic Research Series, Vol. 2.]

————. 1971. Ross Ice Shelf Project. *Antarct. Jnl U.S.*, **6**, No. 6, 258–63.

————., GIOVINETTO, M., KEHLE, R. *and* J. REID. 1960. Deformation of the Ross Ice Shelf near the Bay of Whales, Antarctica. *IGY glaciol. Rep. Ser.*, No. 3, 148 pp.

PLATE I

The "Dalgliesh Ice Stream" at the point where it enters the Brunt Ice Shelf. Air photograph looking south-east, taken at lat. 75° 10′ S., long. 19° 45′ W. and 5,000 m. above sea-level; January 1970. (Photograph by the U.S. Navy.)

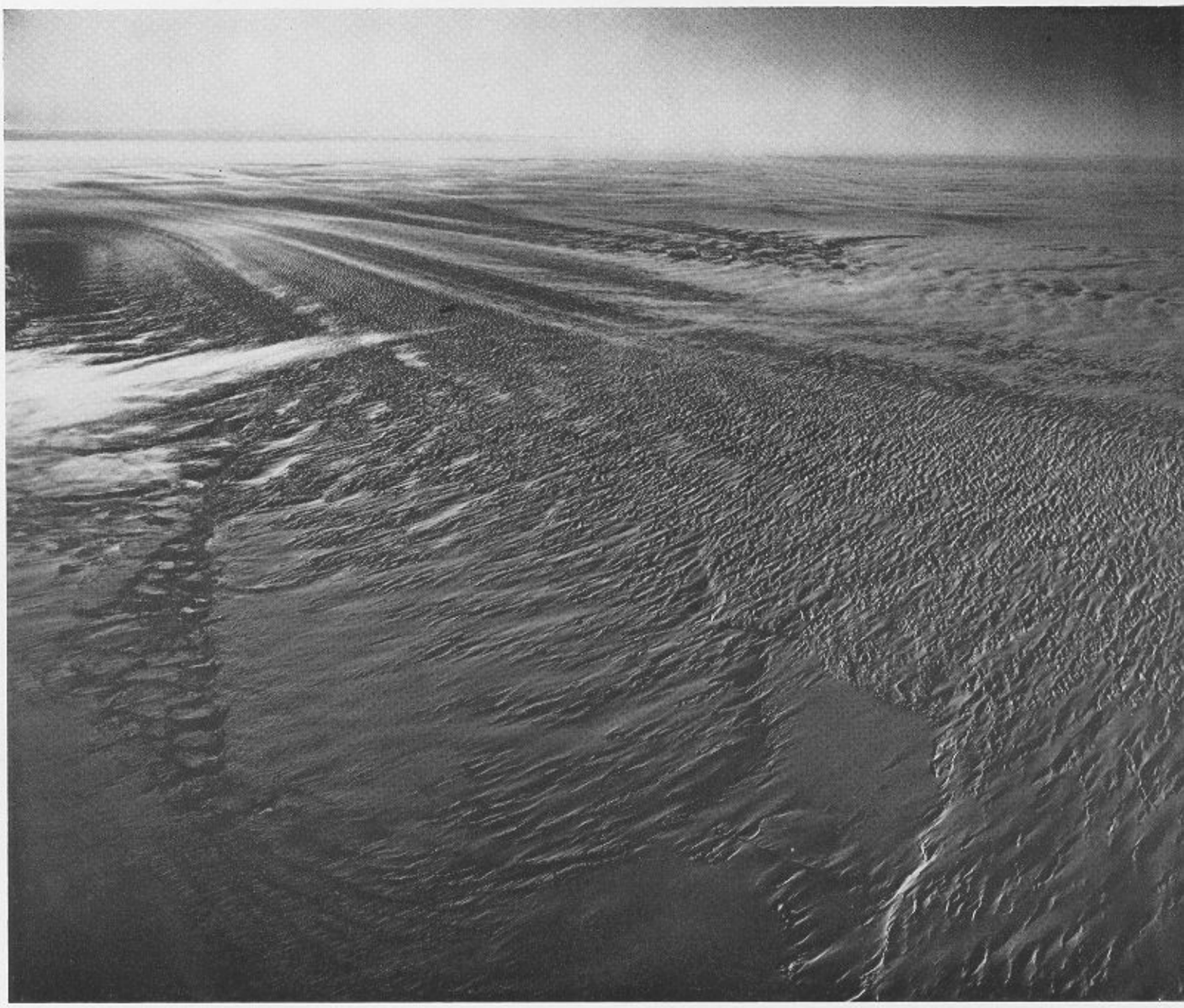

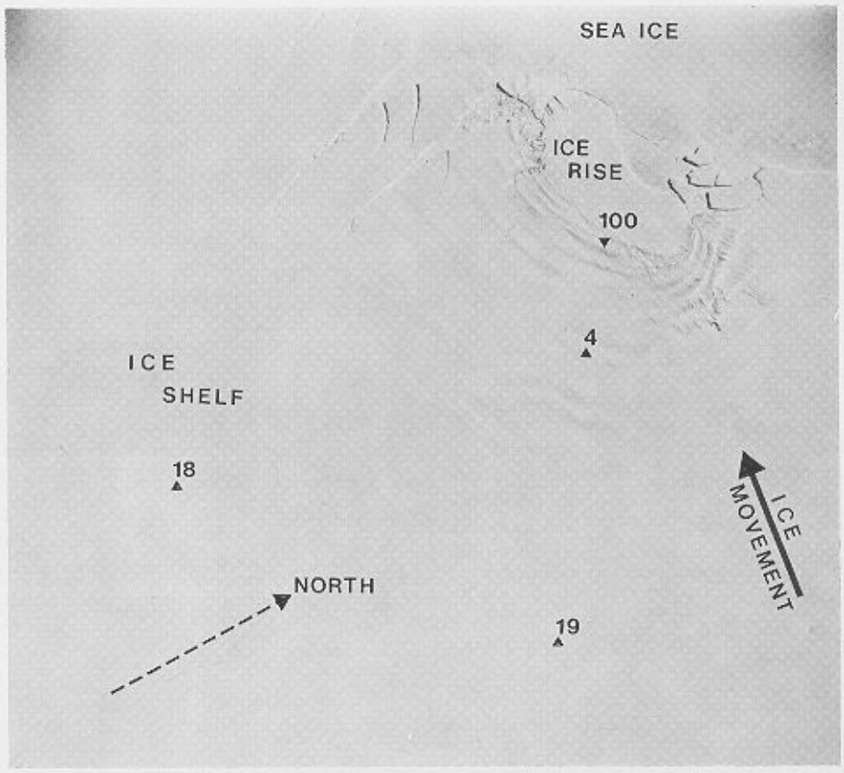
SEA ICE
ICE
RISE
100
4
ICE
SHELF
18
ICE
MOVEMENT
NORTH
19

a

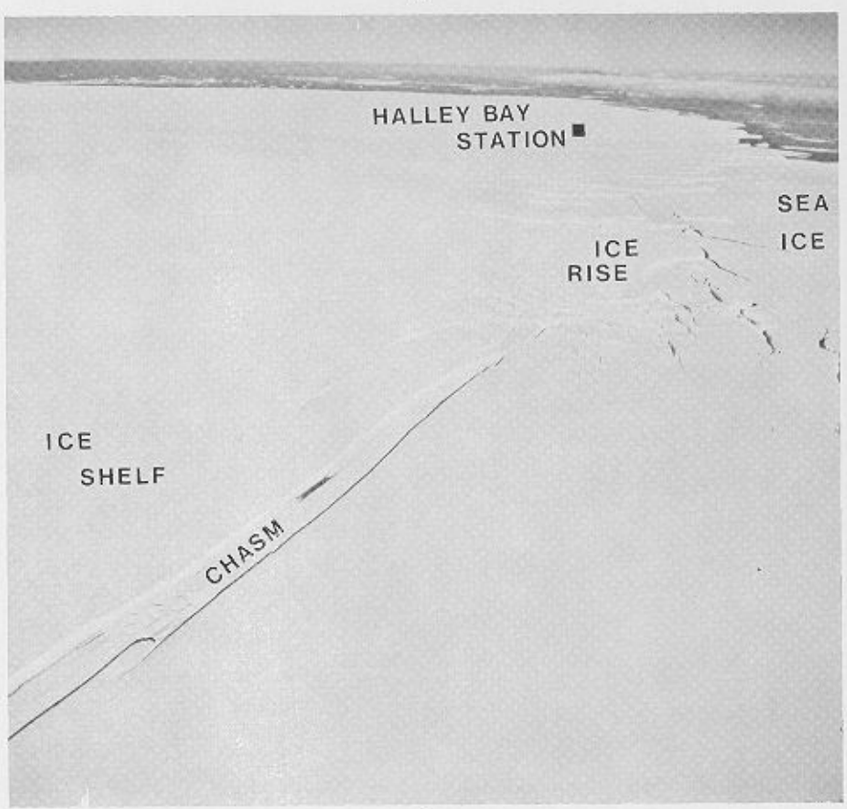
HALLEY BAY
STATION
SEA
ICE
ICE
RISE
ICE
SHELF
CHASM

b

PLATE II

a. Thin ice shelf near R7. Air photograph looking south-east, taken at lat. 75° 20′ S., long. 25° 48′ W. and 8,000 m. above sea-level; December 1967. (Photograph by the U.S. Navy.)

b. Looking south-east along the main stake line; approximate positions of stakes are shown. Air photograph taken at lat. 75° 42′ S., long. 25° 12′ W. and 8,000 m. above sea-level; January 1968. (Photograph by the U.S. Navy.)

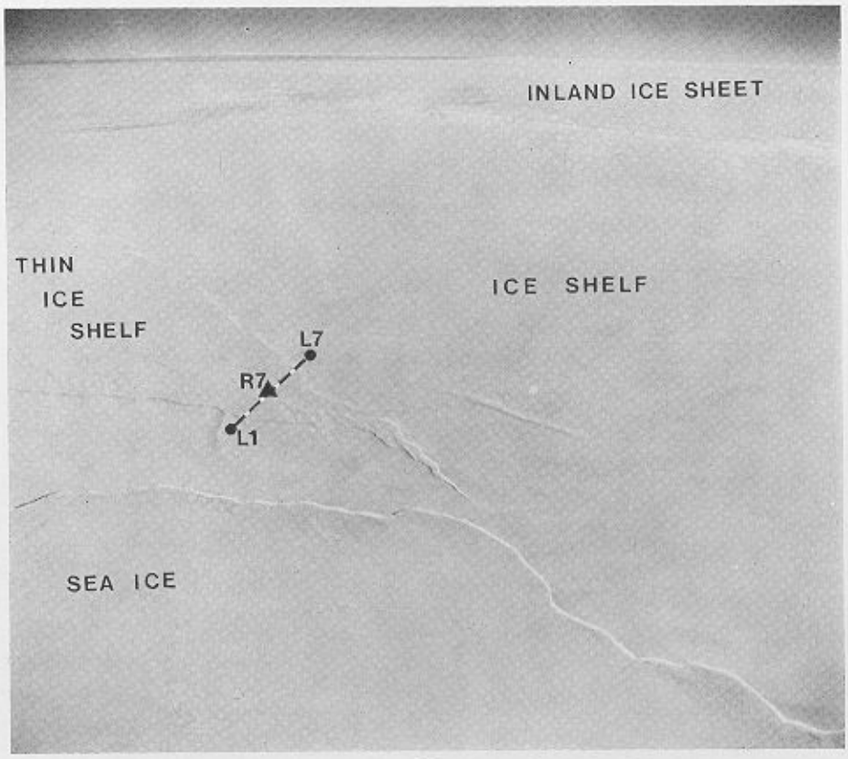
INLAND ICE SHEET
THIN
ICE
SHELF
ICE SHELF
L7
R7
L1
SEA ICE

a

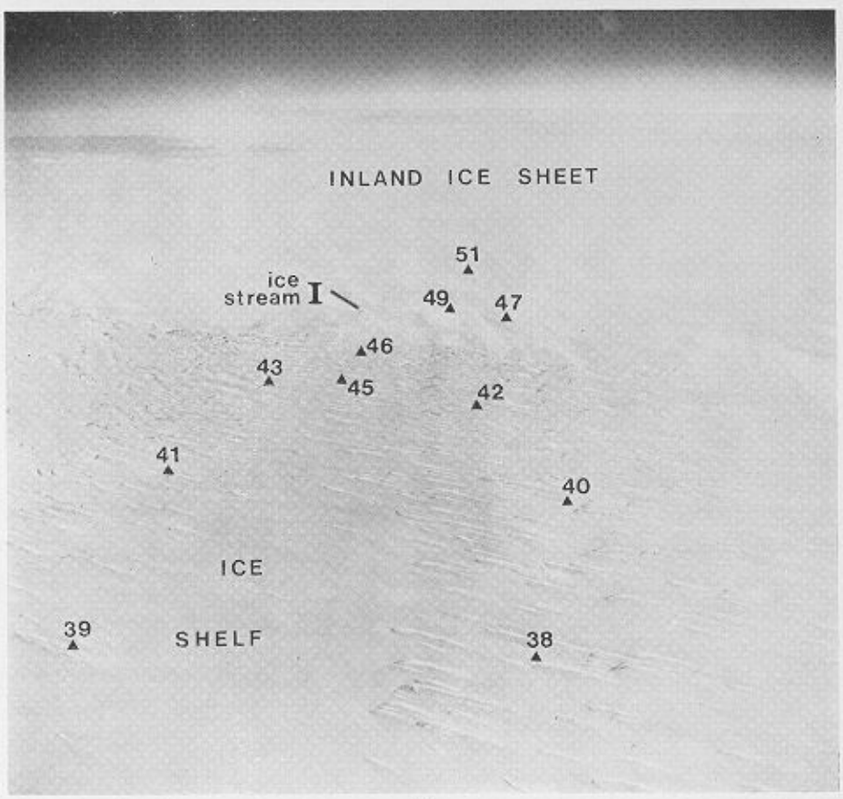
INLAND ICE SHEET
51
ice
stream I
49
47
46
43
45
42
41
40
ICE
39
SHELF
38

b

PLATE III

a. Air photograph taken from 8,000 m. above the McDonald Ice Rumples; December 1967. (Photograph by the U.S. Navy.)

b. Air photograph looking south-west towards the McDonald Ice Rumples, taken at lat. 75° 25′ S., long. 26° 00′ W. and 2,500 m. above sea-level; January 1970. The large chasm in the foreground opened in December 1968. (Photograph by the U.S. Navy.)